Clays and Clay Minerals, Vol. 42, No. 5, 497–517, 1994.

PROGRADE TRANSITIONS OF CORRENSITE AND CHLORITE IN LOW-GRADE PELITIC ROCKS FROM THE GASPÉ PENINSULA, QUEBEC[1]

WEI-TEH JIANG[2] AND DONALD R. PEACOR

Department of Geological Sciences, The University of Michigan
Ann Arbor, Michigan 48109-1063

Abstract—A prograde sequence of corrensite and chlorite in pelitic rocks of the diagenetic zone, anchizone, and epizone (illite crystallinity indices = 0.17–0.58°$\Delta 2\theta$) of the Gaspé Peninsula, Quebec, was studied by analytical and transmission electron microscopy (AEM and TEM). The data collectively suggest that diagenesis/metamorphism of chlorite and corrensite follows a sequence of phase transitions, compositional homogenization, and recrystallization, approaching a state of equilibrium for which chlorite is the stable phase.

Corrensite occurs as coalescing, wavy packets of layers intergrown with chlorite and illite in the diagenetic and low-grade anchizonal rocks. Intergrowths of discrete chlorite and corrensite crystals, interstratified packets of chlorite and corrensite layers, terminations of smectite-like layers by chlorite layers, and 2–3 repeats of R2- and R3-ordered chlorite-smectite mixed layers occur. These materials are alteration products of detrital biotite or other precursor phases like trioctahedral smectite. The crystal size and proportion of corrensite decrease significantly from the diagenetic zone to the anchizone. Deformed corrensite is crosscut by straight packets of chlorite and corrensite in the diagenetic sample. Some chlorite occurs as discrete, euhedral to subhedral crystals intergrown with or enclosed by other phases in the absence of corrensite. The crystal size of chlorite and definition of crystal boundaries increase whereas density of crystal imperfections and randomness in orientation decrease with increase in grade of diagenesis/metamorphism. Crystals that are kinked or bent, or display gliding along (001) form low-angle boundaries with relatively defect-free crystals, implying deformation during crystal growth. Abundant well-defined low-angle boundaries associated with dislocations are observed in the higher grade rocks, consistent with a stage of readjustment of crystal boundaries during crystal growth. The AEM analyses show that the corrensite has lower Fe/(Mg + Fe) and Al/(Si + Al) than the coexisting chlorite in the diagenetic sample, and that the ranges of composition of chlorite of different grades overlap and become smaller with increasing grade, implying prograde homogenization.

The data imply that corrensite is a unique phase that is metastable relative to chlorite: its conversion to chlorite occurred at a grade as low as that of the high-grade diagenetic zone. The textural relations suggest that the metamorphic crystallization and recrystallization were coeval with deformation processes due to tectonism, partially modified by subsequent contact metamorphism. The data, combined with those of previous reports, suggest that the Gaspé Ordovician rocks constitute a part of a regional distribution of trioctahedral phyllosilicate-rich rocks in the northern Appalachians. The regional occurrence of abundant chloritic minerals is thus directly related to a specific tectonic regime with precursor sediments largely derived from an andesitic arc system(s).

Key Words—Analytical electron microscopy, Chlorite, Chlorite crystallinity, Corrensite, Diagenesis, Gaspé Peninsula, Sediment provenance, Syntectonic deformation, Transmission electron microscopy.

INTRODUCTION

Mixed-layer chlorite/smectite (C/S) is the principal clay material that forms under subgreenschist facies conditions in regionally metamorphosed and hydrothermally altered mafic igneous rocks (Alt *et al* 1986, 1989; Bettison and Schiffman 1988; Shau *et al* 1990; Bettison-Varga *et al* 1991; Schiffman and Fridleifsson 1991). It is also common in clastic sedimentary rocks that have been altered by Mg^{2+}-rich fluids or were composed of significant amounts of mafic volcanoclastic materials (April 1981; Vergo and April 1982; Helmold and van de Kamp 1984; Liou *et al* 1985; Chang *et al* 1986; Robinson and Bevins 1986; Weaver 1989; Inoue and Utada 1991). On the basis of X-ray powder diffraction (XRD) data, the smectite-to-chlorite transition has been inferred to occur through the sequence: trioctahedral smectite (saponite) → R0 random C/S → R1 regular C/S (corrensite) → random C/S (high % chlorite without long-range ordering) → chlorite, concurrent with a continuous decrease of expandability (% smectite) with increasing temperature of formation (Evarts and Schiffman 1983; Alt *et al* 1986; Liou *et al* 1985; Chang *et al* 1986; Bettison and Schiffman 1988; Schiffman and Fridleifsson 1991). The sequence, albeit with a lack of long-range ordering, is comparable to the well-known smectite-to-illite transition. However, the sequence of chloritic minerals was

[1] Contribution No. XXX from the Mineralogical Laboratory, Department of Geological Sciences, The University of Michigan, Ann Arbor, Michigan 48109-1063.

[2] Present address: Department of Geology, Arizona State University, Tempe, Arizona 85287-1404.

shown to be discontinuous with steps at 100–80%, 50–40% (corrensite), and 10–0% smectite in a suite of contact metamorphosed rocks and two mineralized areas in northern Japan (Inoue *et al* 1984; Inoue 1985, 1987; Inoue and Utada 1991). The stepwise prograde evolution, the lack of long-range ordering in mixed-layer materials, and the similarity between XRD patterns of random C/S and chlorite/corrensite or corrensite/smectite seem to imply that corrensite is a unique phase rather than a simple mixture of chlorite and smectite layers, and that random C/S (with a low or high percentage of expandable layers) may be a less stable and less common material than corrensite in prograde sequences (Reynolds 1988; Roberson 1988, 1989; Shau *et al* 1990). Ordered interstratification of the smectite component in C/S and the proportion of smectite layers have been shown to be related to the grade of diagenesis and low-grade metamorphism, or to the compositions and thermal history of hydrothermal fluids (Hoffman and Hower 1979; Pollastro and Barker 1986; Kisch 1987; Schiffman and Fridleifsson 1991).

Corrensite or C/S have only rarely been reported to occur in pelitic rocks. They may have been overlooked in some rocks simply because they commonly are not abundant and considered to be insignificant in the diagenesis and metamorphism of pelitic rocks, especially relative to illite. In addition, there are difficulties in identification of such materials by XRD, especially concerning the occurrence of characteristic peaks in the low-2θ region, and peak broadening due to small crystal sizes, lattice strain, and impurities (Reynolds 1988; Moore and Reynolds 1989). Nevertheless, on the basis of an extensive literature survey, Weaver (1989) noted that trioctahedral phyllosilicates such as chlorite and C/S can be as abundant as dioctahedral phyllosilicates in clastic sedimentary rocks, and that trioctahedral phyllosilicates may be indicative of specific sedimentary provenances and tectonic environments. The latter is especially significant, as a general aim of clay mineralogy is to relate clay minerals to broader geological relations.

Although it is difficult to characterize C/S by XRD, it has recently been shown that analytical and transmission electron microscope (AEM and TEM) studies can characterize textures, crystal-chemical relations, and formation processes of C/S in metamorphosed and hydrothermally altered mafic rocks (Shau *et al* 1990; Bettison-Varga *et al* 1991; Shau and Peacor 1992). Although there have been reports of occurrences of expandable chloritic minerals in pelitic rocks based on XRD data, no detailed TEM characterization of C/S in such rocks has been carried out before. The aim of this study, therefore, is to characterize chlorite and C/S in an unusually complete prograde sequence of Ordovician pelitic rocks from the Gaspé Peninsula, Quebec, utilizing TEM and AEM as well as XRD and back-scattered electron (BSE) imaging techniques. Data include the compositions, textures, and structures of trioctahedral chloritic minerals and lead to a definition of formation processes, especially with respect to the relations between metamorphic crystallization and deformation processes. These data, combined with data from previous studies, demonstrate that the trioctahedral chlorite and C/S were derived from a specific type of detrital source involving an andesitic arc system.

MATERIALS AND EXPERIMENTAL TECHNIQUES

The Gaspé Peninsula is part of the northern Appalachian mountain belt. The Taconic Orogeny is the earliest of three major deformation events that affected the area, involving diachronous collision of the eastern continental margin of North America (Laurentia) with an island arc system(s) during late Cambrian and Ordovician time (St. Julien and Hubert 1975; Williams and Hatcher 1983). A complex foreland basin was created through the loading of an imbricate thrust system that consisted of the obducted forearc accretionary prism and volcanic arc(s) on to the thin North American lithosphere (St. Julien and Hubert 1975; Williams and Hatcher 1983; Quinlan and Beaumont 1984; Pickering 1987). These obducted materials formed the principal sources for Ordovician clastic sediments filling the foreland basin. Pelites collected in this study are from the middle Ordovician (Llandelian-Caradocian) Deslandes Formation (~2.3 km thick) of deep-marine basin-floor turbidites and the middle to late Ordovician (Caradocian-Ashgillian) Cloridorme Formation (~4.0 km thick) of basin-floor turbidites and submarine-fan deposits formed in the foreland basin, overlying the foundered Cambrian carbonate platform and platform-derived clastic turbidite sequences (Enos 1969; Pickering and Hiscott 1985; Hiscott *et al* 1986; Pickering 1987). Both the Deslandes and Cloridorme Formations contain thick sequences of alternating shales and coarser clastic rocks. The Deslandes Formation and earlier-deposited foreland-basin turbidite systems were thrust over the younger Caradocian-Ashgillian systems, initially coeval with deposition of the Cloridorme Formation (Pickering 1987).

Structurally, the Taconic belt has been subdivided into an autochthonous domain, an external domain comprising an outer belt of thrust-imbricated structure and an inner belt of emplaced nappes, and an internal domain (St. Julien and Hubert 1975). The internal domain consists of highly deformed and metamorphosed rocks (Shickshock Group of Cambrian age, Figure 1), partly overlying Precambrian continental crust and oceanic crust. The external domain which includes the Tourelle Formation, Cap des Rosiers Group, and Deslandes Formation of the inner belt, and the Cloridorme Formation, was metamorphosed to a much lesser extent. These stratigraphic units were folded and over-

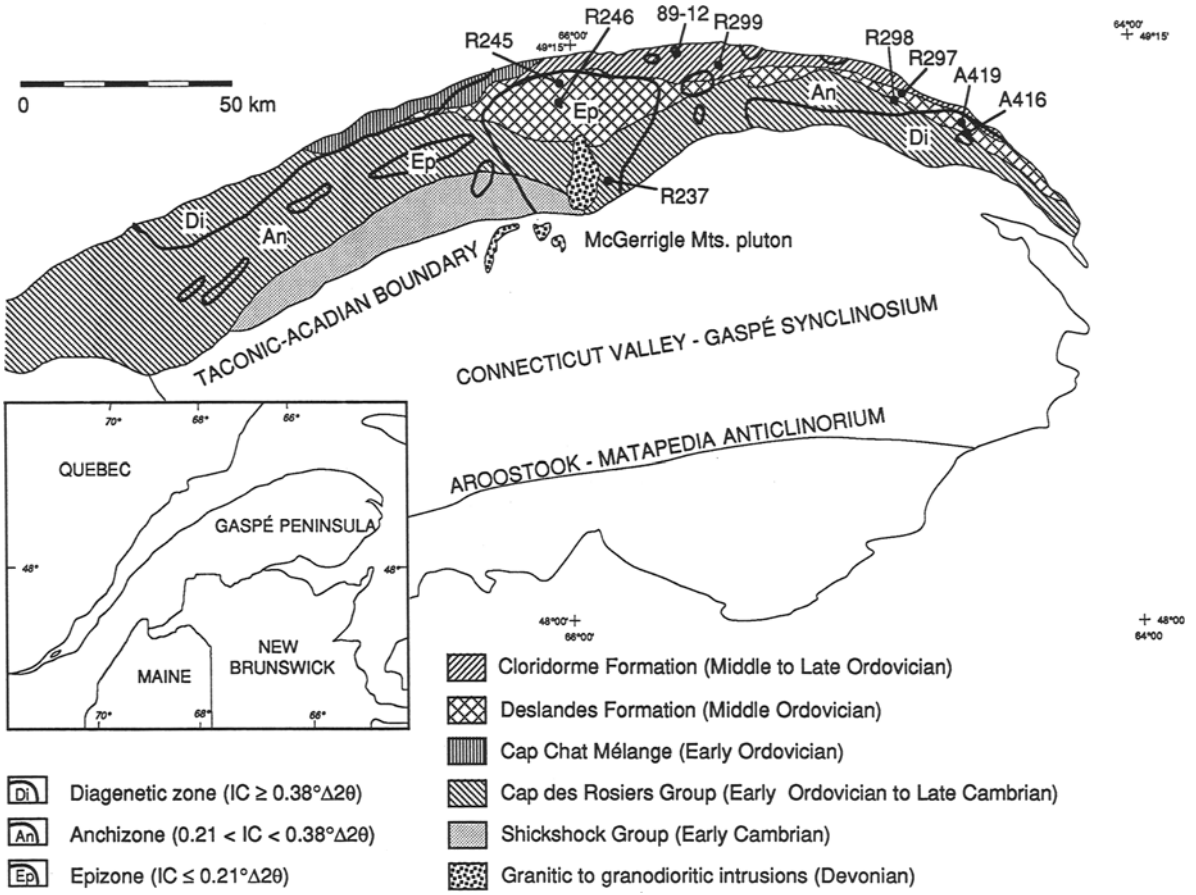

Figure 1. Geological map showing the stratigraphy and the pattern of regional diagenesis and low-grade metamorphism of the pelitic rocks in the Taconic belt of the Gaspé Peninsula, Quebec (modified after Hesse and Dalton 1991). Sample localities are indicated by small solid circles tied to sample identifications with straight lines.

thrust by lateral compression during the Taconic Orogeny. The dynamothermal metamorphism was completed at ~440 Ma (St. Julien and Hubert 1975). Subsequent orogenic activity had little or no effect on these rocks. The unfoliated granitic to granodioritic McGerrigle pluton (Figure 1) was subsequently emplaced during Upper Devonian time (Whalen 1985), resulting in a local increase in metamorphic grade due to contact metamorphism.

A prograde sequence of nine pelitic rocks located within the Taconic orogenic belt along the northern coast of Gaspé Peninsula was selected for this study (Figure 1). The rocks were selected so that samples represented a large range of illite crystallinity, the prograde sequence is continuous and as well defined as possible, and the dioctahedral phyllosilicates include only the smectite-muscovite sequence with no complications due to Na-bearing white micas. The samples either were collected from the same formation or at least can be shown to be petrographically similar.

Regional patterns of the degree of diagenesis and low-grade metamorphism of pelitic rocks in the Gaspé Peninsula were defined by Islam *et al* (1982), Duba and Williams-Jones (1983), Islam and Hesse (1983), and Hesse and Dalton (1991). Islam *et al* (1982) observed a simple regional pattern with an increase of diagenetic and metamorphic grade toward the McGerrigle pluton due to thermal alteration, superimposed on a northward trend of increasing grade that parallels a decrease in rock ages in the area east of the pluton. The inverse relation between metamorphic grades and rock ages reflects the Taconic tectonic influence. The zone of diagenesis, as well as the anchizone and epizone, were mapped on the basis of illite crystallinity and vitrinite reflectance values. Hesse and Dalton (1991) synthesized all available data relating to the pelitic rocks, defining the regional diagenetic/metamorphic pattern of the Taconic and Acadian belts in the Gaspé Peninsula. The pattern in the Taconic belt was more or less the same as that reported by Islam *et al* (1982), but the values of illite crystallinity index were calibrated in order to be consistent with the data from other regions in the Peninsula. The resulting values were much larger (poorer crystallinity) than those of

https://doi.org/10.1346/CCMN.1994.0420501 Published online by Cambridge University Press

Table 1. Illite crystallinity indices and chlorite/illite wt. % ratios of the studied pelitic samples (ethylene glycol solvated <2 μm fractions) from the Gaspé Peninsula, Quebec.

Samples	Illite crystallinity index	Diagenetic/ metamorphic grade[1]	Chlorite/ illite[2]
A419	0.58°Δ2θ	Diagenetic zone	0.54
A416	0.45°Δ2θ	Diagenetic zone	0.49
R297	0.36°Δ2θ	Anchizone	0.37
R298	0.31°Δ2θ	Anchizone	0.34
R299	0.31°Δ2θ	Anchizone	0.68
89-12	0.27°Δ2θ	Anchizone	0.32
R237	0.25°Δ2θ	Anchizone	0.48
R245	0.19°Δ2θ	Epizone	0.35
R246	0.17°Δ2θ	Epizone	0.47
Average			0.45

[1] The limits for the anchizone are 0.21 and 0.38°Δ2θ based on Kisch's standard set (Kisch 1990).

[2] Wt. % ratios obtained with integrated intensities of ~7 and ~5 Å peaks and calibration curves established with standards.

Islam *et al* (1982). The illite crystallinity indices of the samples used in the present study were measured in our laboratory and shown to have values (Table 1) lower than those estimated from the zonal pattern defined by Hesse and Dalton (1991). A set of interlaboratory correlation samples for illite crystallinity measurements (Kisch 1990) were therefore used in order to calibrate the limits of the anchizone. We obtained values nearly identical to those of Kisch for his samples. The diagenetic/metamorphic grades of the studied samples were therefore redefined (Table 1) on the basis of Kisch's limits (0.38 and 0.21°Δ2θ) for the anchizone. The pattern shown in Figure 1 uses Kisch's limits instead of those defined by Hesse and Dalton (1991). The temperatures of diagenesis and metamorphism of the region were estimated to be ~80°C in the diagenetic zone and ~260°C in the epizone based on fluid inclusion data (Islam and Hesse 1983; Hesse and Dalton 1991).

Significant variations in illite crystallinity index values occur among rocks from the anchizone in the Deslandes Formation. The variations are probably due to local alteration initiated by fluids associated with faults (Islam *et al* 1982). Samples R297, R298, and R299 (low-grade anchizone) and 89-12 (high-grade anchizone) of the Cloridorme Formation were therefore chosen as intermediate samples between the diagenetic and epizonal rocks of the Deslandes Formation. The Deslandes and Cloridorme Formations were effectively deposited in the same environment. The pelitic rocks in both formations have similar compositions and mineral assemblages and were metamorphosed largely during regional tectonic activity, and locally by thermal metamorphism, rather than by burial diagenesis prior to the Taconic Orogeny.

Both powdered bulk rocks and <2 μm (equivalent spherical diameter) fractions of all nine samples were analyzed by XRD. The <2 μm fractions were obtained by sedimentation of disaggregated samples in distilled water and oriented specimen slides were prepared by a pipette method (Brown and Brindley 1984). Ethylene-glycol solvation of the <2 μm fractions was carried out by vaporizing ethylene glycol in a vacuum desiccator at room temperature. XRD patterns were obtained on air-dried and ethylene glycol-solvated specimens of the <2 μm fractions with CuKα radiation at 35 kV and 15 mA using a Philips XRD 3100 X-ray generator. A theta compensating slit, a receiving slit of 0.2 mm, a Soller slit assemblage, a graphite crystal monochromator, and a scintillation detector are fitted on the diffractometer. A step size of 0.01°Δ2θ and a counting time of ~6 seconds per step were used in order to obtain high quality patterns. Quartz occurs in all samples and was used as an internal standard for 2θ corrections. All patterns were digitally recorded and processed on a microprocessor. Interpretation of the patterns was based on Reynolds (1984), Moore and Reynolds (1989), Środoń (1984), and Tomita *et al* (1988). Crystallinity indices were obtained by measures from the widths at half height of the basal reflections of illite and chlorite without corrections for instrumental broadening.

Preparation of TEM specimens was detailed in Jiang and Peacor (1991). Carbon-coated, ion-milled TEM specimens were first studied by optical microscopy and scanning electron microscopy (SEM) to identify large-scale textural relations and to locate areas of interest for TEM observations. All SEM images shown here are BSE images. A Philips CM12 scanning transmission electron microscope equipped with a low-angle Kevex Quantum detector for X-ray energy-dispersive spectroscopy analyses was used for TEM imaging, electron diffraction, and AEM analyses. Instrumental settings and characterization procedures were described in Jiang *et al* (1992), Slack *et al* (1992), and Jiang and Peacor (1993).

X-ray powder diffraction

The XRD patterns of the air-dried and ethylene glycol-solvated specimens of the <2 μm fractions of samples A416 and R299 are given in Figure 2 as examples for the diagenetic and low-grade anchizonal rocks, respectively. The XRD pattern of the air-dried <2 μm fraction of sample A416 consists of peaks with d-values of 14.37, 7.12, and 4.76 Å; the d-values and relative intensities are abnormal for 00*l* reflections of pure chlorite. After ethylene-glycol solvation, the 14.37-Å reflection shifted to a lower 2θ position corresponding to d = 15.21 Å with a shoulder skewed toward the high 2θ side. The 7.12-Å reflection split into two overlapping components with d-values of 7.11 and 7.51 Å, respectively. The 4.98-Å peak of illite displayed a tail on the low 2θ side after glycol solvation due to the displacement of the mixed-layer component of the

broad 4.76-Å reflection. These changes suggest that the chloritic material consists of an expandable C/S component and a non-expandable chlorite component. The presence of the 29.40- and 31.58-Å superlattice reflections in the XRD patterns of the air-dried and glycol-solvated samples, respectively, is consistent with the presence of R1 ordering (i.e., a corrensite component) in the C/S. The breadth of the superlattice reflections is caused by variations of the chlorite/smectite ratio from the ideal value of 50:50, and perhaps in part to the small average crystal size, high lattice strain, and/or heterogeneous composition of the mixed-layer material (Moore and Reynolds 1989). The mixed-layer component is identified as C/S with ~60% chlorite and R1 ordering based on the aforementioned features and peak positions. After heating at 375°C, a significant decrease in the intensity of the ~14-Å reflection is associated with the addition of a high-2θ shoulder, and the 7.51-Å reflection like that shown in Figure 2 was shifted further toward the low 2θ side in patterns of the diagenetic samples (Jiang 1993), typical of the characteristics of C/S (Bettison and Schiffman 1988; Schiffman and Fridleifsson 1991). In the pattern of the air-dried specimen, the ~10-Å peak of illite is slightly asymmetric and has a tail on the low 2θ side. The width at half height of the peak decreases after glycol solvation. These features imply the presence of a small proportion of expandable mixed layers in illite.

The patterns of the anchizonal sample R299 obtained before and after glycol solvation are nearly the same except for a small decrease in half-height widths of the chlorite peaks that become slightly asymmetric, as typical of the presence of expandable layers interstratified with chlorite. However, there are no apparent differences in peak positions from those of normal chlorite. These data imply that sample R299 consists largely of chlorite but with a small component of C/S. The XRD patterns of other anchizonal samples have similar features.

The XRD patterns of the epizonal rocks (not shown) display no indication of mixed layering and have peaks that are much narrower than those of samples from lower grades. The only peaks of phyllosilicates are those of muscovite and chlorite with the exception of very weak peaks of talc that were detected locally in the epizonal rocks.

The Gaspé rocks contain relatively abundant chloritic minerals compared to pelitic rocks in the Acadian and Alleghenian clastic wedges (e.g., Catskill Formation, Martinsburg Formation, Chattanooga Shales, etc.) (Faill 1985; Conkin 1986; Lee *et al* 1986; Rheams and Thornton 1988). Table 1 shows the chlorite-to-illite weight concentration ratios of the clay fractions of the pelites studied herein. These values were determined using integrated intensities and calibration curves established with standards. The average concentration ratio is 0.45, much larger than the average value of

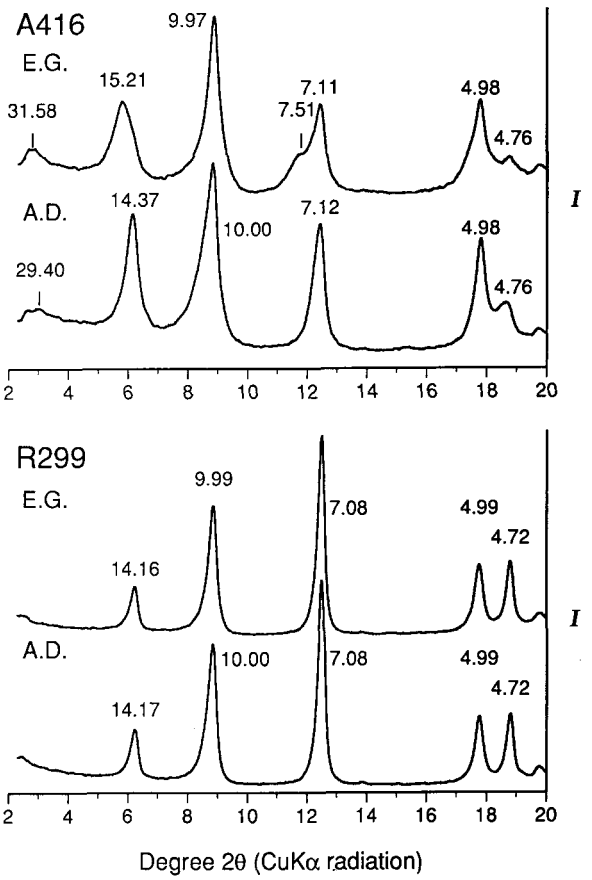

Figure 2. X-ray powder diffraction patterns of the <2 μm fractions (E.G. = ethylene glycol solvated and A.D. = air dried) of sample A416 of the diagenetic zone and sample R299 of the low-grade anchizone. Labeled numbers are d values in Å.

0.20 obtained for shales and slates from other localities in North America (Weaver 1989).

The chlorite crystallinity indices (half-height widths of ~7- and ~14-Å reflections) of both the air-dried and ethylene glycol-solvated samples were measured and plotted against the corresponding illite crystallinity indices (measured on the ethylene glycol-solvated samples) in Figure 3. The illite and chlorite crystallinity indices show a strong correlation for all samples except for the ethylene glycol-solvated samples of the diagenetic rocks (samples A416 and A419). The chlorite crystallinity index values of the low-grade anchizonal and high-grade diagenetic rocks increased significantly because the chlorite reflections overlap with the displaced reflections of C/S after ethylene glycol solvation. The 7-Å chlorite crystallinity index values did not change as much as the 14-Å values after glycol solvation because the peaks split into separate components. The 7-Å chlorite crystallinity indices appear to be slightly smaller than the 14-Å chlorite crystallinity indices of the anchizonal samples as a result of the

https://doi.org/10.1346/CCMN.1994.0420501 Published online by Cambridge University Press

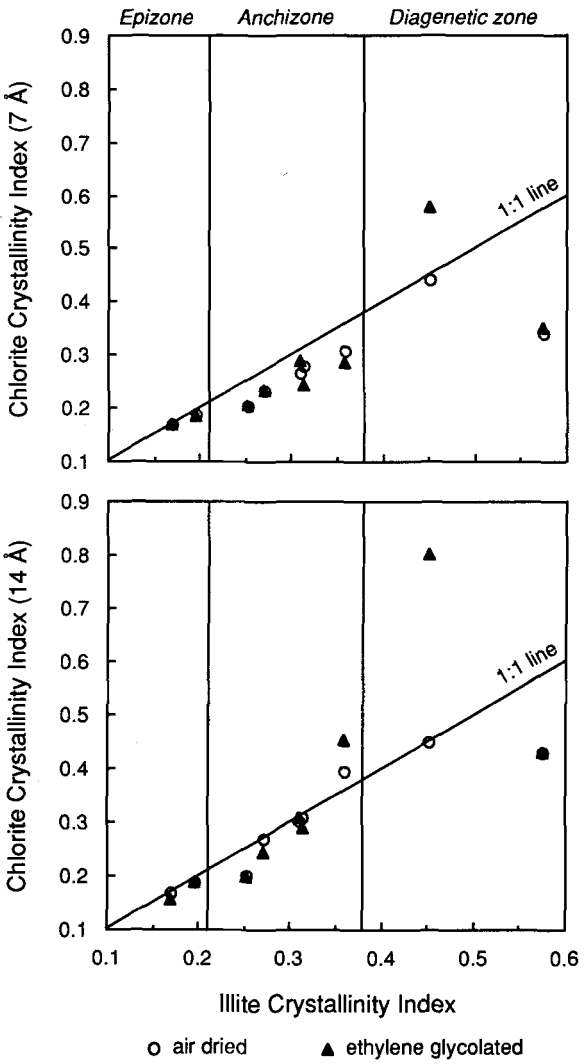

Figure 3. Illustrative plots showing the correlation between the illite crystallinity indices (ethylene glycol solvated) and chlorite crystallinity indices (O = air dried; ▲ = ethylene glycol solvated) of the pelites from the Gaspé Peninsula.

presence of serpentine-type mixed layers (Slack *et al* 1992). Peaks for the lowest grade rock (sample A419 having the largest value of illite crystallinity index) did not show much change after glycol solvation because there is not much C/S in the fine-grained fractions. Instead, there is much more coarse-grained, slightly-altered detrital biotite than in sample A416, the latter having abundant C/S. The illite crystallinity index of sample A419 is large because of the presence of illite-rich mixed-layer illite/smectite, resulting in a large deviation of the data points from the 1:1 reference line.

Petrographic observations

The mineral assemblages of the studied samples are summarized in Table 2. The principal diagenetic/metamorphic changes of minerals other than those described in the section above include alteration of detrital biotite, prograde evolution of $1M_d$ illite to 2M muscovite, albitization of plagioclase and potassium feldspar, and reaction of titanite + fluid to yield quartz + calcite + anatase (rutile in the epizonal rocks) (Jiang 1993).

Table 2. Constituent minerals of the pelitic rocks from the Gaspé Peninsula.

Samples	Minerals
A416, A419 (Diagenetic zone)	corrensite, chlorite, $1M_d$ illite, illite/smectite, quartz, plagioclase, albite, potassium feldspar, calcite, apatite, anatase, titanite, magnetite, biotite, paragonite, zircon, Cr,Ni,Fe spinel
R297, R298, R299 (Anchizone)	corrensite, chlorite, $1M_d$ and $2M_1$ illite, muscovite, quartz, albite, potassium feldspar, calcite, anatase, pyrrhotite, pyrite, titanite, apatite
89-12, R237 (Anchizone)	chlorite, illite ($2M_1$ dominated), muscovite, quartz, albite, calcite, anatase, pyrrhotite, pyrite, apatite, talc
R245, R246 (Epizone)	chlorite, muscovite, quartz, albite, calcite, rutile, pyrite, pyrrhotite, magnetite, apatite, talc

The phyllosilicates occur as aggregates of very fine-grained crystals in the matrix of the diagenetic samples (often not resolvable by SEM), surrounding coarser grained minerals, principally quartz, albite, and detrital biotite and forming a foliation parallel to the bedding (Figure 4a). In BSE observations, the areas that consist of C/S commonly have irregular microfissures that probably were generated by dehydration in the SEM vacuum, and have minor alkali and Ca contents and relatively high Si contents compared to normal chlorite. Such clays occur only rarely in the low-grade anchizonal samples.

In the low-grade anchizonal sample R299, the phyllosilicates appear to be coarser grained and more grains have outlines that are relatively well defined (Figure 4b) as compared with those in the diagenetic rocks. The quartz and albite grains are less angular than their diagenetic equivalents. There is a weak cleavage parallel to the bedding.

The high-grade anchizonal samples have been deformed in response to tectonic stress as evidenced by the presence of highly distorted chlorite-mica stacks (Figure 4c). The orientations of fine-grained clay minerals appear to be partially rearranged, giving rise to a poorly defined foliation subparallel to the bedding.

Two planar fabrics are present in the epizonal samples. The first is bedding, which is defined by quartz and albite-rich (≤ 1 cm thick) and thin calcite-rich (≤ 1

https://doi.org/10.1346/CCMN.1994.0420501 Published online by Cambridge University Press

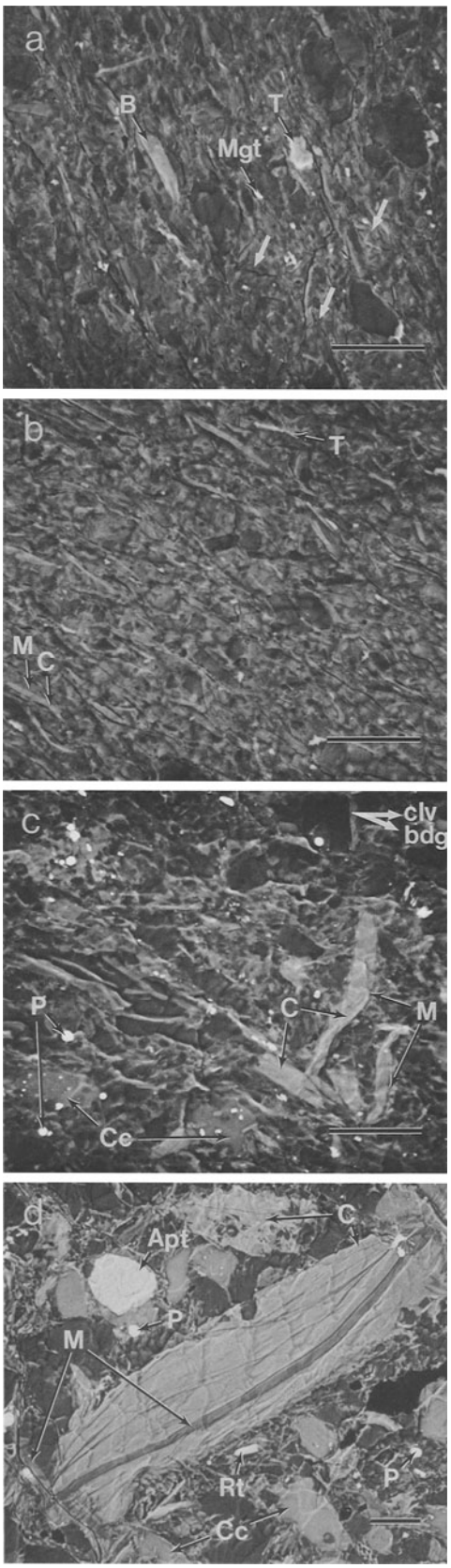

mm thick) lamellae. Most of the lamellae are deformed to some extent. There are some large deformed chlorite-muscovite stacks (15–50 μm in thickness) having their long aspect parallel or subparallel to the bedding. The second fabric is the foliation of fine-grained chlorite and muscovite, forming an anastomosing spaced cleavage subnormal to the bedding. Dark grey lenticular domains ($\leq$1 cm thick) having a relatively high concentration of fine-grained phyllosilicates and light-grey, elongated regions consisting largely of quartz, albite, and calcite are dispersed throughout the anastomosing spaced cleavage. An example of the relatively phyllosilicate-rich domains in sample R245 is shown in Figure 4d. The long aspect of the large chlorite-muscovite stack is normal to the cleavage. Fine-grained phyllosilicates are parallel or subparallel to cleavage except in areas where the orientations of the phyllosilicates are constrained by quartz and albite grains. Most muscovite and chlorite grains have well-defined boundaries and are larger than their lower grade equivalents.

Transmission electron microscope observations

Five pelites (A419, A416, R299, 89-12, and R245) that are representative of the sequences in minerals and textures were chosen for TEM study. The data presented here were all obtained from the fine-grained matrices of the samples as shown above in BSE images.

Diagenetic zone. Figure 5 shows a few coalescing bundles of fringes that have ~24-Å periodicity, display layer curvature and dislocations (layer terminations), and give a series of diffuse 00*l* reflections with d-values corresponding to a phase with ~24-Å periodicity. These features are characteristic of corrensite, consisting of ordered chlorite-like (14 Å) and dehydrated, collapsed

←

Figure 4. Back-scattered electron images of ion-milled samples A416 (a), R299 (b), 89-12 (c), and R245 (d). All scale bars represent a length of 20 μm. Irregular grains with dark contrast are quartz or albite. (a) Three corrensite-rich areas, exhibiting irregular microfissures, are highlighted with white arrows. The matrix consists mainly of very fine-grained corrensite, chlorite, and illite. B = biotite; T = titanite; Mgt = magnetite. (b) The matrix consists of the same assemblage as that in (a). C = chlorite; T = titanite; M = K-rich white mica. (c) The directions of the bedding (bdg) and cleavage (clv) are indicated with white arrows. Relatively large phyllosilicate grains (labeled with M and C) in the lower-right are deformed. The matrix minerals include chlorite, illite, and very fine-grained anatase (with bright contrast). C = chlorite; Cc = calcite; M = K-rich white mica; P = pyrite or pyrrhotite. (d) The long aspect of the large chlorite-muscovite stack in the middle is normal to the cleavage. The matrix phyllosilicates are muscovite and chlorite commonly associated with fine-grained rutile (irregular small grains with bright contrast). C = chlorite; M = muscovite; Cc = calcite; Rt = rutile; Apt = apatite; P = pyrite or pyrrhotite that are partially altered to form magnetite.

https://doi.org/10.1346/CCMN.1994.0420501 Published online by Cambridge University Press

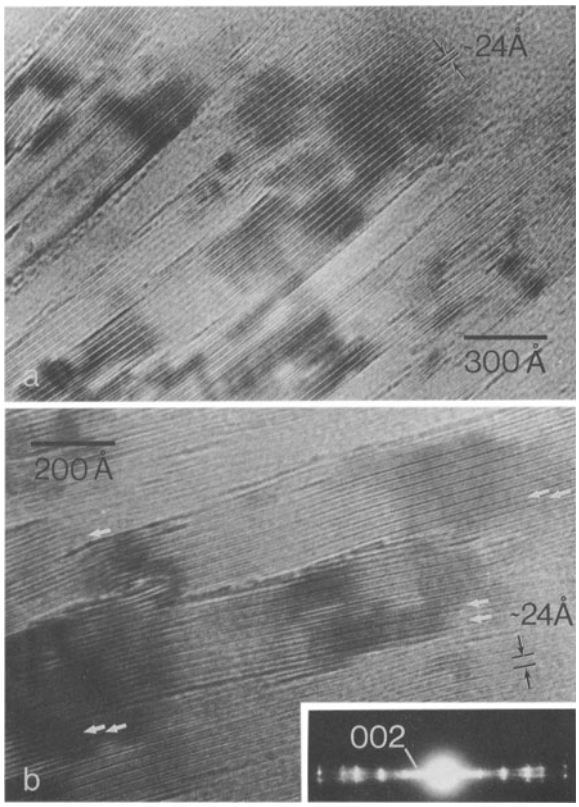

Figure 5. Lattice-fringe images of corrensite in sample A416 of the diagenetic zone, obtained with (a) the (001) plane slightly oblique and (b) the (001) plane parallel to the electron beam. (a) Lacks sub-fringes but displays coalescing packets of layers with ~24-Å periodicity. (b) Shows ~24-Å layers with sub-fringes. A few chlorite layers are indicated by white arrows. d(002) ≅ 12 Å.

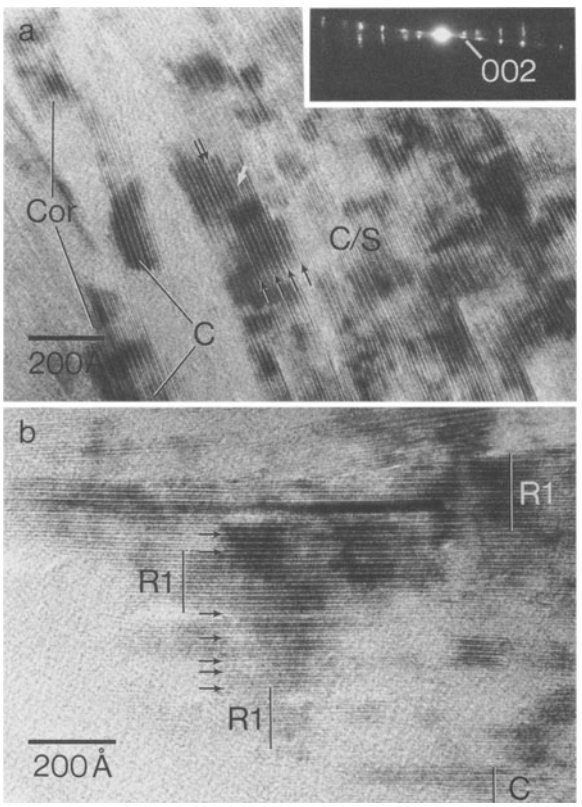

Figure 6. Lattice-fringe images of mixed-layer chlorite/smectite (or chlorite/corrensite) in sample A416. (a) Mixed-layer chlorite/smectite (C/S) intergrown with discrete packets of chlorite (C) and corrensite (Cor). Three repeats of R2-ordered mixed-layer chlorite/smectite units (marked by black arrows) are associated with a termination of a collapsed ~10-Å smectite layer by a ~14-Å chlorite layer (highlighted with a white arrow) and two successive smectite layers in the middle. The corresponding electron diffraction pattern shows irrational 00*l* reflections associated with streaking along c*. d(002) ≅ 12 Å. (b) Packets of R1-ordered mixed-layer chlorite/smectite interstratified with one R2-ordered and two R3-ordered units of mixed-layer chlorite/smectite (highlighted with black arrows), and chlorite, forming a thick stack of mixed-layer chlorite/smectite with R1 ordering or random mixed-layer chlorite/corrensite.

smectite-like (10 Å) layers. A few chlorite ~14-Å layers are interstratified with packets of corrensite in Figure 5b. Such corrensite packets commonly occur in aggregates coexisting with discrete chlorite crystals. The thickness of individual corrensite packets varies from ≤1000 Å as discrete crystals to ~24 Å as single layers interstratified with chlorite. Some clay aggregates consist of three discrete components including chlorite, corrensite, and a material consisting of complex mixed layers with many ~10-Å layers separated by one or more ~14-Å layers (Figure 6a). The latter material can be interpreted to be chlorite-rich C/S with R1 ordering or as mixed-layer chlorite/corrensite. Three repeats of R2-ordered C/S units that may also be described as mixed-layer chlorite/corrensite with R1 ordering occasionally occur (Figure 6a). Termination of a ~10-Å layer by a ~14-Å layer is also present. Two or three repeats of R3-ordered C/S or R2-ordered mixed-layer chlorite/corrensite were also detected (Figure 6b). Such complex mixed layering must be a principal cause of the poor definition of corrensite reflections in XRD patterns. An interesting texture in which a folded corrensite stack is crosscut at the fold hinge by straight packets of corrensite and chlorite having well-defined crystal boundaries and interlocking relations is shown in Figure 7.

In addition to the intergrowths with corrensite, chlorite also occurs as packets of layers intergrown with illite, generally in the absence of corrensite, as shown in Figure 8a. The stack of chlorite layers in the middle of the image has two fringes with different contrast due to the presence of ~7-Å layers (presumably berthierine). Such mixed layers occur only rarely in the sample. A small packet of layers is bent against the edges of the layers of the adjacent crystal, forming a low-angle

https://doi.org/10.1346/CCMN.1994.0420501 Published online by Cambridge University Press

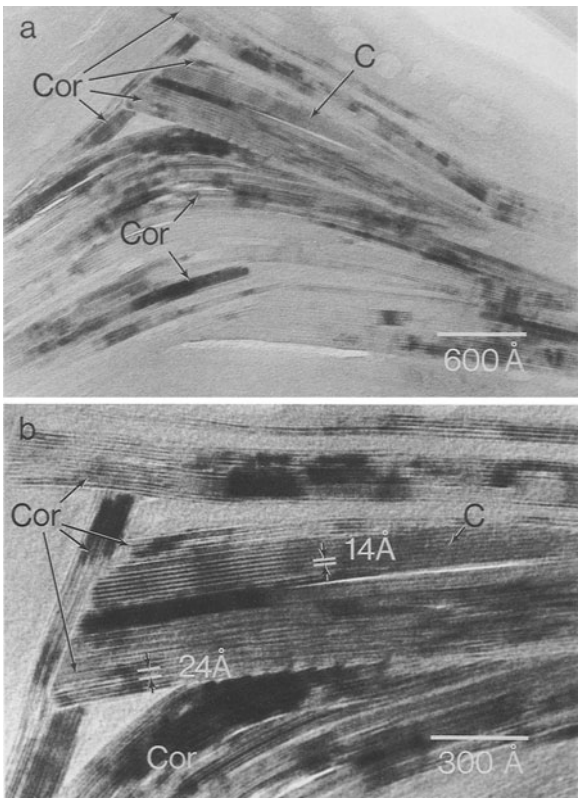

Figure 7. (a) TEM image of chlorite (C) and corrensite (Cor) showing deformation and interlocking textures in sample A416. The deformed corrensite is crosscut by straight packets of corrensite and chlorite. (b) An enlargement of (a).

boundary that continues with a ~7-Å layer. That texture implies that mechanical rotation (intra- and intercrystal gliding) occurred while crystallization proceeded. The diagenetic chlorite also occurs as euhedral to subhedral crystals intergrown with or enclosed by other phases (Figure 8b). Corrensite rarely occurs in the vicinity of this type of crystal. Such crystals commonly have fewer defects than does corrensite.

Low-grade anchizone. Corrensite is much less common in the low-grade anchizonal samples. It occurs as thin packets (≤300 Å thick) of layers interstratified with packets of chlorite (occasionally also with illite) that vary widely in thickness, the combined packets forming thick stacks (Figure 9). Discrete, thick packets of corrensite were rarely observed. In general, chlorite layers tend to cluster together forming relatively thick packets of layers. Such a feature is exemplified in Figure 9a in which a thin packet of corrensite and several isolated corrensite (or smectite) layers are interstratified with relatively thick packets of chlorite. Consecutive ~10-Å smectite layers such as those shown in the middle of Figure 9a occur only rarely in the low-grade anchizonal sample. Some smectite layers ter-

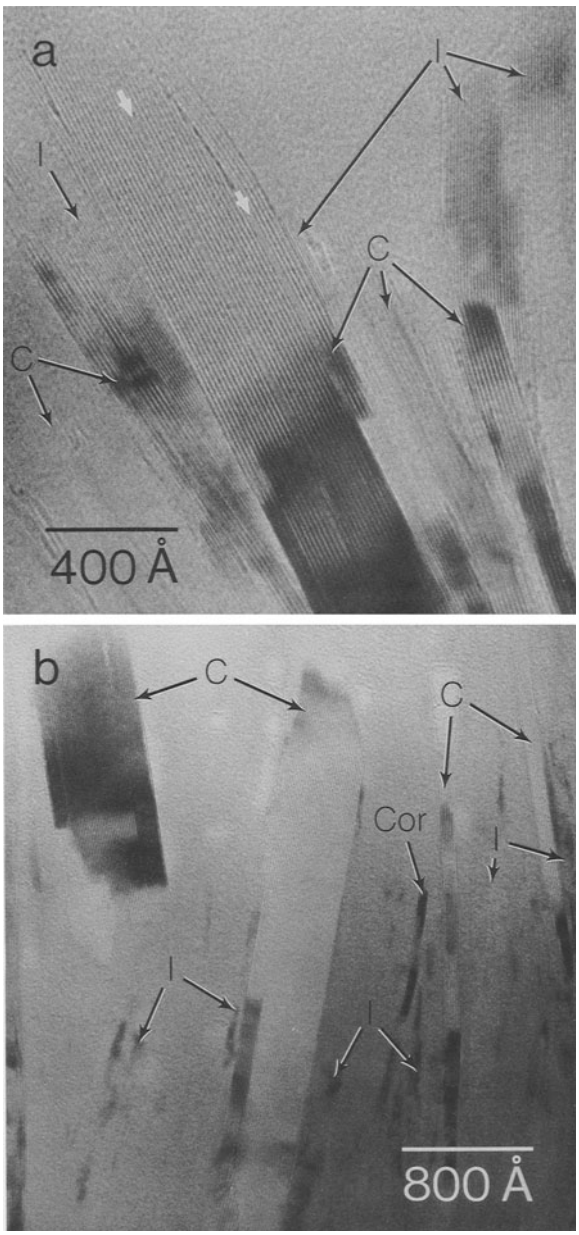

Figure 8. Lattice-fringe images of illite-chlorite intergrowths in the diagenetic sample A416 showing (a) interlocking relations between illite (I) and chlorite (C) and buckling of chlorite layers against the edges of the adjacent crystal, two ~7-Å layers (highlighted with white arrows) occurring in the large chlorite crystal in the center, and (b) euhedral to subhedral chlorite crystals intergrown with illite with little or no deformation features. Corrensite (Cor) occurs rarely in such intergrowths.

minate against chlorite layers, as consistent with progressive replacement of smectite layers by chlorite. The corresponding electron diffraction pattern shows streaking and irrational reflections along c* in addition

https://doi.org/10.1346/CCMN.1994.0420501 Published online by Cambridge University Press

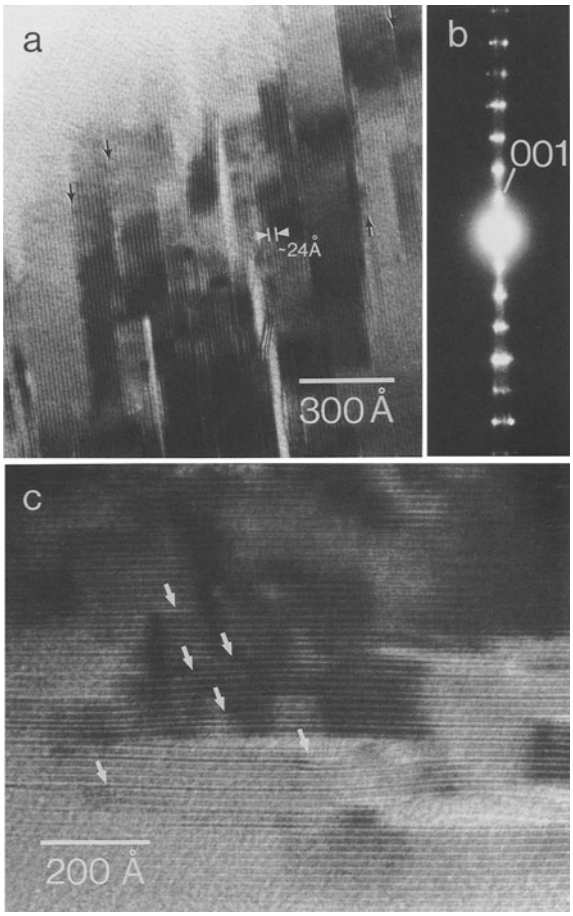

Figure 9. (a) Lattice-fringe image of packets of chlorite interstratified with thin packets of mixed-layer chlorite/smectite (or chlorite/corrensite) in sample R299 of the low-grade anchizone. Single smectite (or corrensite) layers (marked with black arrows) are locally associated with terminations by chlorite layers (wide fringes). A small packet of corrensite and three instances of successive smectite layers (narrow fringes) occur in the center. (b) Electron diffraction pattern of (a) showing 00*l* reflections of chlorite superimposed on irrational reflections and streaking along c*. d(001) ≅ 14 Å. (c) Lattice-fringe image of complex mixed layers between ~14-Å layers of chlorite (wide fringes) and ~10-Å layers of smectite (narrow fringes) or ~24-Å layers of corrensite. Terminations of layers are marked by white arrows.

to the sharp 00*l* reflections of chlorite, consistent with the presence of discrete chlorite and mixed layering.

Thin packets of corrensite tend to be interstratified with small numbers of chlorite layers, the assemblage thus constituting disordered (R = 0) mixed-layer chlorite/corrensite or chlorite-rich C/S with R1 ordering. Terminations of ~10-Å fringes by ~14-Å fringes are more common in the low-grade anchizonal sample than in the diagenetic samples, implying that the anchizonal mixed layers represent a transition stage. Even numbers of consecutive ~14-Å fringes and terminations of

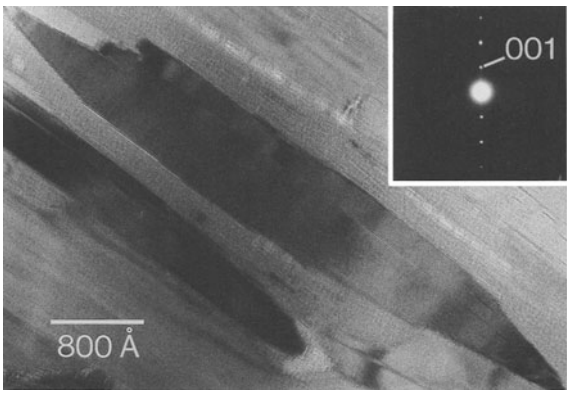

Figure 10. TEM image of chlorite crystals in the low-grade anchizonal sample R299, showing step-like crystal boundaries and straight fringes with no mixed layers and no obvious deformation features. The corresponding electron diffraction pattern shows sharp 00*l* reflections with virtually no streaking. d(001) ≅ 14 Å.

smectite by chlorite in opposite directions in adjacent layers are not uncommon, as exemplified by Figure 9a.

Well-defined chlorite crystals are much more abundant in the low-grade anchizonal sample, as compared with samples from the zone of diagenesis. Such crystals are elongated and display straight, well-defined lattice fringes with no mixed layering, and give only sharp 00*l* reflections in electron diffraction patterns (Figure 10). In many cases, chlorite crystals have step-like boundaries in contact with the surrounding clay crystals, many of which do not give lattice fringes, probably because their (001) planes were not parallel to the electron beam. Chlorite-illite intergrowths and discrete, euhedral to subhedral chlorite crystals similar to those in the diagenetic rocks (e.g., Figure 8) are common, but have a larger average crystal size.

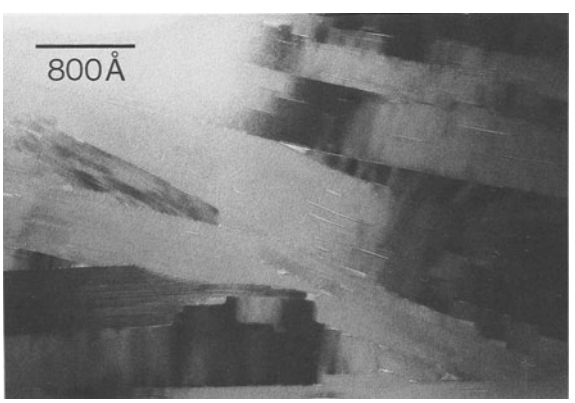

Figure 11. TEM image of an aggregate of subparallel packets of chlorite displaying interlocking textures with virtually no pore space between crystals in sample 89-12 of the high-grade anchizone.

https://doi.org/10.1346/CCMN.1994.0420501 Published online by Cambridge University Press

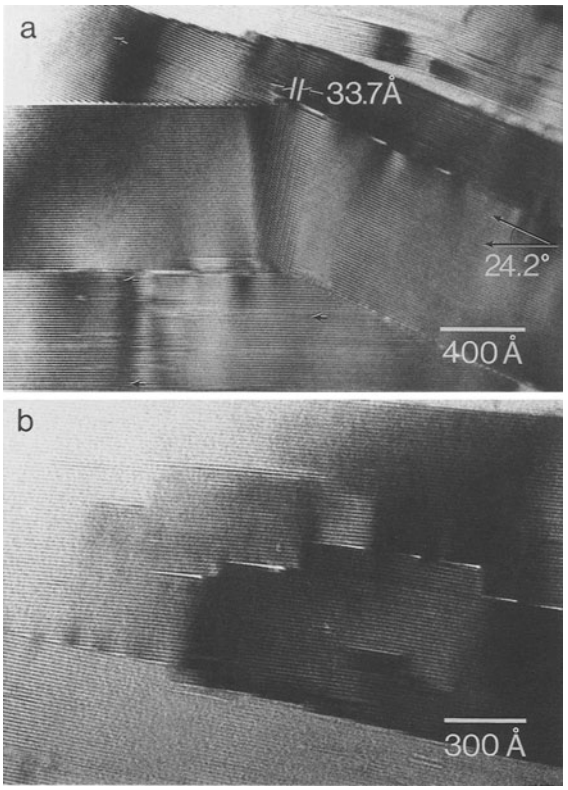

Figure 12. Lattice-fringe images of chlorite in sample 89-12 of the high-grade anchizone. (a) A kinked crystal is surrounded by relatively undeformed crystals. The moiré fringes with a spacing of ~33.7 Å in the center are due to overlapping of two domains twisted with respect to each other by an angle of ~24.2°. A few ~7-Å layers (marked by black arrows) occur in the surrounding crystals. (b) A low-angle boundary is associated with several dislocations in a stack of packets of chlorite.

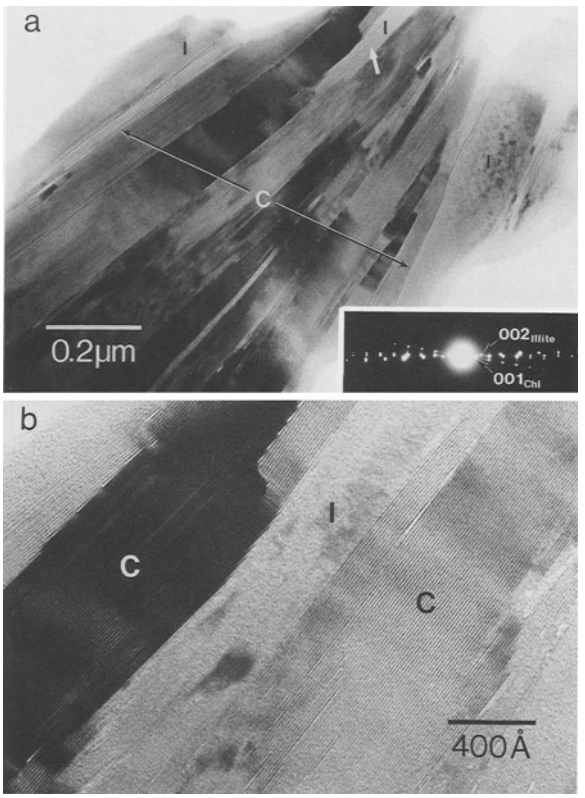

Figure 13. (a) TEM image of a chlorite-illite intergrowth in sample 89-12 showing subparallel packets of chlorite (C) and illite (I) related by low-angle boundaries. The inset is an electron diffraction pattern obtained from part of the region, showing non-parallel 00*l* reflection rows of chlorite and illite. The 002 reflection of illite (indexed on the basis of a two-layer polytype) and 001 reflection of chlorite have d-values of ~10 Å and ~14 Å, respectively. (b) An enlargement of the illite area marked by a white arrow in (a) showing intracrystal bending and kinking in chlorite. The illite area lacks some lattice fringes due to partial damage by the electron beam.

High-grade anchizone. No corrensite or C/S was observed in sample 89-12 of the high-grade anchizone. The high-grade anchizonal chlorite commonly occurs as aggregates of subparallel packets of layers that display lattice fringes over relatively large areas, compared with those occurring in the lower grade rocks, implying parallelism of layers (with respect to the electron beam) over relatively large volumes. Figure 11 shows an aggregate of subparallel packets of chlorite for which there is virtually no pore space between crystals, as crystal outlines are largely constrained by adjacent crystals. Some chlorite packets occurring in such aggregates contain contrasting deformation features.

A kinked crystal that is surrounded by relatively undeformed crystals is shown in Figure 12a. The moiré fringes in the kinked crystal have a spacing of ~33.7 Å that satisfies the equation for the magnification of a 'rotation moiré pattern' (Hirsch *et al* 1977), $M = D/d = 1/[2 \sin(\alpha/2)]$, where D = the spacing of moiré fringes, d = the original spacing of the crystals, and α = the angle by which the crystals are twisted with respect to each other. The moiré fringes therefore were formed by overlapping of two domains that have an identical spacing (assumed to be 14.1 Å) and that were twisted with respect to each other by an angle of ~24.2°. There are a few serpentine-type ~7-Å fringes, presumably berthierine, in the surrounding chlorite crystals. Such ~7-Å layers were occasionally observed in rocks of all grades.

Chlorite crystals in some packets of this kind of aggregate display abundant low-angle boundaries and dislocations (Figure 12b). Illite packets often are a component of this type of aggregate, and Figure 13a shows a stack of layers consisting of subparallel packets of chlorite and illite. One of the illite crystals (highlighted by a white arrow) does not penetrate but has low-angle boundaries with the chlorite crystals. A lattice-fringe image (Figure 13b) of that highlighted region shows

https://doi.org/10.1346/CCMN.1994.0420501 Published online by Cambridge University Press

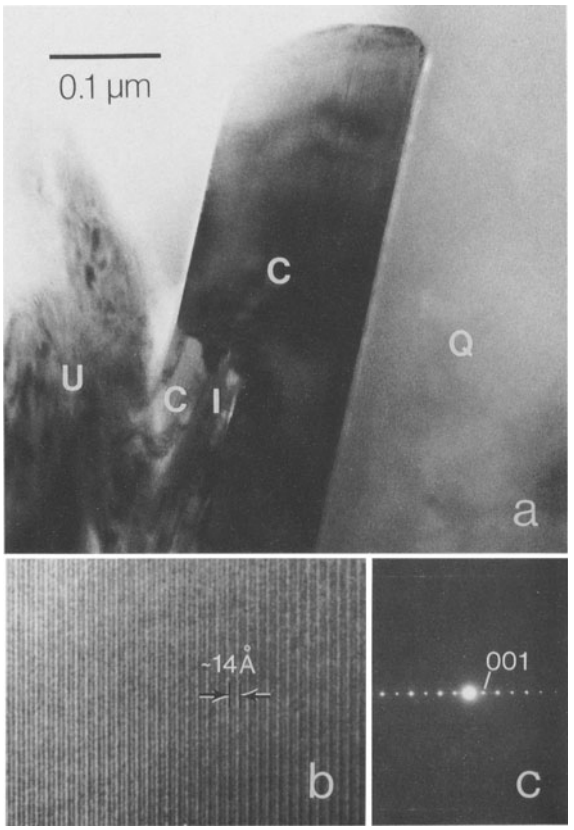

Figure 14. (a) TEM image of a euhedral crystal of chlorite in sample 89-12 with no obvious deformation features. C = chlorite; Q = quartz; I = illite; U = unidentified. (b) Lattice-fringe image of part of the euhedral chlorite crystal in (a) showing no mixed layering. (c) Electron diffraction pattern of the euhedral crystal in (a) displaying continuous streaking in 24*l* (or its pseudohexagonal equivalents) reflection rows. d(001) ≅ 14 Å.

that kinking and/or bending occurred within some of the chlorite crystals, resulting in the formation of intracrystal low-angle boundaries or arrays of dislocations. The illite region in Figure 13b actually consists of several subparallel packets of layers without any obvious deformation features.

Chlorite-illite stacks with much smaller crystal sizes similar to those observed in the lower grade rocks were also observed. Well-developed euhedral crystals of chlorite occur in the high-grade anchizonal sample as well, commonly adjacent to or included within recrystallized quartz or albite, as in the lower grade rocks. This type of chlorite crystal is relatively perfect and usually has no deformation features (Figure 14). Electron diffraction patterns of chlorite from all studied samples show continuous streaking in non-00*l* ($k \neq 3n$) reflection rows (Figure 14), implying a semi-random stacking sequence (Bailey 1988).

Epizone. Crystal size increases significantly from the anchizone to the epizone, small crystals being rare in the epizonal sample. Aggregates of well-defined, large chlorite or muscovite crystals are dominant. Euhedral crystals without defects are abundant. However, crystal defects, including dislocations, stacking faults, kinking, slip along (001), and bending occur in some of the large crystals. Small crystals commonly have fewer defects and are intergrown with large deformed or undeformed crystals.

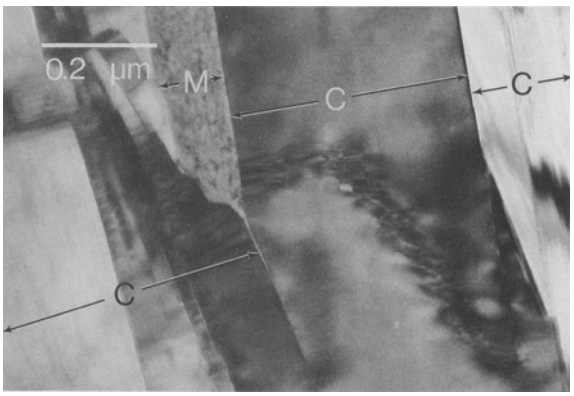

Figure 15. TEM image of an assemblage of chlorite (C) and muscovite (M) crystals in sample R245 of the epizone. The large chlorite crystal in the middle-left contains clusters of dislocations running across the (001) plane of which the trace is subnormal to the black arrows. The adjacent crystals are relatively defect-free.

A collection of chlorite and muscovite crystals in sample R245 of the epizone is shown in Figure 15. A wedge-shaped chlorite crystal in the middle that has clusters of dislocations running across the (001) plane is surrounded by several relatively defect-free crystals. Such a crystal probably was in a final stage of recrystallization during which defects caused by early deformation were partially eliminated.

Analytical electron microscope analyses

Tables 3 and 4 show representative AEM analyses of corrensite and chlorite. The analyses were normalized to 20 O + 16 OH and 20 O + 10 OH for chlorite and corrensite, respectively. More than half of ~300 analyses were discarded because analyzed areas contained mixed layering or other phases such as albite, illite, or quartz, as verified by electron diffraction and lattice-fringe imaging. Inclusion of more than one mineral in analyses occurred mainly for diagenetic samples because crystals were smallest in that sample. Only 19 acceptable analyses were obtained for the diagenetic chlorite.

All chlorite formulae have nearly equal numbers of tetrahedral and octahedral Al and nearly complete trioctahedral occupancy. The Al/(Si + Al) ratio is nearly constant regardless of the grade of diagenesis/metamorphism. However, the Fe/(Mg + Fe + Mn) ratio of

https://doi.org/10.1346/CCMN.1994.0420501 Published online by Cambridge University Press

Table 3. Representative normalized analytical electron microscope data for corrensite in pelites from the diagenetic zone and low-grade anchizone of the Gaspé Peninsula.[1,2]

	Diagenetic zone					Low-grade anchizone		
	1	2	3	4	5	6	7	8
Si	5.71	5.80	5.39	5.97	5.93	5.70	5.59	5.86
Al	3.91	3.79	4.22	3.59	3.50	4.00	3.94	4.01
Mg	4.19	4.02	4.34	4.33	4.19	4.21	4.46	3.75
Fe	3.19	3.38	3.12	2.92	3.26	3.23	3.27	3.35
Mn	0.13	0.13	0.07	0.03	0.01	0	0	
Tet. + Oct.	17.13	17.12	17.14	16.84	16.89	17.14	17.26	16.97
K	0.14	0.11	0.31	0.26	0.29	0.07	0.06	0.08
Na	0.07	0.11	0.19	0.26	0.24	0.25	0.11	0.24
Ca	0.11	0.07	0.11	0.17	0.17	0	0.10	0
Interlayer charge[3]	0.43	0.36	0.72	0.86	0.87	0.32	0.37	0.32
$\frac{Fe}{Mg + Fe + Mn}$	0.42	0.45	0.42	0.40	0.44	0.43	0.42	0.47
$\frac{Al}{Si + Al}$	0.41	0.40	0.44	0.38	0.37	0.41	0.41	0.41

[1] Normalization is based on 20O + 10OH and all Fe is assumed to be ferrous.

[2] Two standard deviations on the basis of counting statistics are 0.15–0.18 pfu (per formula unit) for Si, 0.13–0.15 pfu for Al, 0.14–0.16 pfu for Mg, 0.07–0.08 pfu for Fe, 0.03–0.04 pfu for K, 0.01–0.03 pfu for Na, and ≤0.02 pfu for Ca and Mn.

[3] Interlayer charge is calculated from the total charge originated from Ca and alkali contents that normally are assigned to the interlayer site of smectite.

chlorite varies widely, particularly in the lower grade rocks, largely within the range 0.23–0.68. The octahedral Al content ranges from 2.1 to 3.1 per $O_{20}OH_{16}$. The Al/(Si + Al) ratio of ~0.50 is relatively high compared with that of most chlorite in mafic rocks (Bevins *et al* 1991), reflecting the higher bulk-rock Al content of pelitic rocks. All analyses contain minor Mn, but Ti (≤0.02 per formula unit), Ca, or alkalis (Σ(Ca + alkalis) ≤ 0.05 pfu) are only rarely detected at the trace level. No specific correlation between the composition and texture or structure of the chlorite was detected, nor is there any systematic variation in composition with grade.

The analyses of the diagenetic and low-grade anchizonal corrensite were obtained from areas that were dominated by corrensite but that occasionally contained minor chlorite layers and very rarely had consecutive smectite-like layers. The totals of tetrahedral and octahedral cations of formulae for Gaspé corrensite (Table 3) are all close to 17, as typical of corrensite (Brigatti and Poppi 1984). The Fe/(Mg + Fe + Mn) and Al/(Si + Al) ratios of ~0.43 and ~0.40 are nearly constant among all analyses, but the interlayer charges originating from the smectite-like component of corrensite vary from ~0.3 to ~0.9 (Table 3). The formulae have variable K, Na, Ca, and Mn contents, but the interlayer K, Na, and Ca contents are each of the same order of magnitude in most formulae. The low-grade anchizonal corrensite appears to have a smaller net negative charge than does the diagenetic corrensite but the total number of analyses is small and therefore such comparisons may not be valid.

Table 4. Representative normalized analytical electron microscope data for chlorite in low-grade pelitic rocks from the Gaspé Peninsula.[1,2]

	Si	Al	Mg	Fe	Mn	$\frac{Fe}{Mg + Fe + Mn}$	$\frac{Al}{Si + Al}$
Diagenetic zone							
Sample A419							
1	5.41	5.17	4.62	4.64	0.16	0.49	0.49
2	5.34	5.33	3.37	5.81	0.17	0.62	0.50
3	5.38	5.24	4.89	4.30	0.18	0.46	0.49
Sample A416							
4	5.48	5.05	3.56	5.88	0.04	0.62	0.48
5	5.27	5.45	4.60	4.57	0.10	0.49	0.51
6	5.30	5.41	4.97	4.25	0.08	0.46	0.51
Anchizone							
Sample R299							
7	5.26	5.66	3.05	5.81	0.14	0.65	0.52
8	5.49	4.94	6.07	3.49	0.06	0.36	0.47
9	5.34	5.32	4.81	4.44	0.09	0.48	0.50
Sample 89-12							
10	5.36	5.28	3.92	5.28	0.16	0.56	0.50
11	5.33	5.26	5.25	4.11	0.08	0.44	0.50
12	5.41	5.27	4.50	4.73	0.04	0.51	0.49
Epizone							
Sample R245							
13	5.42	5.14	5.35	4.04	0.08	0.43	0.49
14	5.27	5.57	4.08	4.94	0.09	0.54	0.51
15	5.46	5.18	5.10	4.11	0.11	0.44	0.49

[1] Normalization is based on 20O + 16OH and all Fe is assumed to be ferrous.

[2] Two standard deviations on the basis of counting statistics are 0.14–0.17 pfu (per formula unit) for Si and Al, 0.12–0.18 pfu for Mg, 0.07–0.12 pfu for Fe, and 0.01–0.03 for Mn.

https://doi.org/10.1346/CCMN.1994.0420501 Published online by Cambridge University Press

DISCUSSION

Relation between the abundance of trioctahedral phyllosilicates and tectonic environment

The studied rocks document a well-defined prograde sequence of trioctahedral phyllosilicates progressing in part from detrital material that included volcanic biotite to corrensite to chlorite. Such a sequence has been only rarely described in pelitic rocks (Frey 1978; Weaver *et al* 1984; Robinson and Bevins 1986), for which chlorite commonly has been inferred to form as a by-product of the smectite-to-illite reaction or from alteration of kaolinite or berthierine (Hower *et al* 1976; Boles and Franks 1979; Ahn and Peacor 1985; Walker and Thompson 1990). Dioctahedral phyllosilicates such as illite or muscovite are usually present in amounts much greater than those of trioctahedral minerals in shales, commonly reflecting the presence of either dioctahedral smectite as an original detrital phase as in Gulf Coast sediments, or volcanic ash that was subsequently altered to form dioctahedral smectite. By contrast, C/S is common in altered intermediate to mafic igneous rocks, reflecting the high concentration of Mg in those rocks relative to the high Al content of most pelites. The presence of C/S in clastic rocks implies that original detrital material had a significant intermediate to mafic volcanogenic component (Helmold and van de Kamp 1984; Chang *et al* 1986; Roberts and Merriman 1990). Because the composition of volcanic material may vary in a predictable way in response to tectonic setting, the occurrence of pelitic rocks with abundant trioctahedral phyllosilicates may be diagnostic of that origin.

In Quebec, the abundance of chlorite increases from the Lower and Middle Ordovician to Upper Ordovician rocks in the St. Lawrence Lowlands (Dean 1962). In western Newfoundland, Suchecki *et al* (1977) documented the occurrence of diagenetic corrensite and mixed-layer illite/smectite in the late Lower to Middle Ordovician rocks, in contrast to the occurrence of 2M illite-rich sediments in the Middle Cambrian to early Lower Ordovician rocks of the Cow Head Breccia. They suggested that such a change was caused by the Taconic Orogeny, which transformed the sediment provenance from that of cratonic rocks to volcanic arc rocks. Enos (1969) suggested that the sediments in the Cloridorme Formation of the Gaspé Peninsula originated from an island arc system based on the presence of volcanic debris and paleocurrent information inferred from fossil distributions and sedimentary structures and facies. The occurrence of corrensite and the relatively high concentration of chloritic minerals in the studied rocks may therefore reflect the tectonic setting of the Ordovician pelitic rocks in the Taconic belt of the Gaspé Peninsula, with a significant proportion of detrital sediments having been transported from an Ordovician island arc system. Such a correlation is consistent with the distributions of chlorite-rich (including C/S) rocks and bentonites in Ordovician rocks on two sides of the Proto-Atlantic (Iapetus) Ocean (Weaver 1989).

The detrital Cr, Ni, Fe spinel (an intermediate chromite-nichromite solid solution) and titanian biotite identified by Jiang (1993) provide evidence of the relatively mafic volcanic materials derived from the island arc system that has been inferred (Enos 1969; Pickering 1987). Jiang (1993) showed that the corrensite and chlorite in the Gaspé rocks were largely alteration products of detrital titanian biotite of volcanic origin. The fine-grained matrix minerals consist in part of dioctahedral illite or mixed-layer illite/smectite in the diagenetic rocks, with textures as consistent with alteration from smectite that, presumably, was derived from volcanic glass either *in situ* or prior to deposition. The high proportion of matrix corrensite and chlorite is also inferred to have had an origin in detrital biotite and glass or smectite; however, alteration of Mg,Fe-bearing volcanogenic materials would give rise to both dioctahedral and trioctahedral components, as demonstrated for chlorite coexisting with mixed-layer illite/smectite in Gulf Coast sediments by Ahn and Peacor (1985, 1986). All these data collectively indicate that a significant contribution of relatively mafic volcanogenic material was the cause of the relatively high concentration of chloritic minerals in the pelitic rocks of the Gaspé Peninsula.

The presence of abundant detrital titanian biotite in the diagenetic rocks implies that the volcanic source contained a significant portion of andesitic material having a relatively high volatile content that typically occurs in island arc systems located along ocean-continent converging margins (Hyndman 1985). This is consistent with the tectonic setting of the Taconic belt. The associated materials in the island arc-accretionary prism complex, including pelagic sediments, ophiolitic rocks, clastic rocks, and volcanic ash, may have provided additional materials as the source of other detrital materials such as spinel, muscovite, potassium feldspar, plagioclase, quartz, and volcanic glass necessary for the formation of dioctahedral (and possibly trioctahedral) smectite in the Gaspé rocks. The studied Gaspé rocks that contain relatively high concentrations of chloritic minerals must therefore be part of a regional distribution of chlorite-rich rocks with sediments largely derived from an ancient volcanic arc system. Other pelitic sequences that were derived largely from deposition of felsic volcanics or alkali-rich continental clastics, e.g., Gulf Coast sediments (Hower *et al* 1976), the delta argillites of the Belt Supergroup, Idaho (Eslinger and Sellars 1981), the Mowry and Skull Creek shales of the Rocky Mountains (Burtner and Warner 1986), and the epicontinental shales of the Campos basin, Brazil (Anjos 1986), do not contain abundant corrensite or chloritic minerals. The Gaspé rocks thus represent a special type of pelitic sequence involving

deposition of abundant andesitic volcanics derived from an island arc system. Pelites deposited in other back-arc basins, such as the Lower Paleozoic rocks of Wales (Robinson and Bevins 1986) and Oslo Region (Björlykke 1974) similarly contain abundant C/S and/or chlorite. Such rocks may be precursors to chlorite-rich rocks free of C/S by regional or contact metamorphism as is the case in the Gaspé rocks.

Overview of prograde sequence

The relations described above imply that the original sediments were composed of a significant andesitic volcanic component. In the samples of the diagenetic zone, Jiang (1993) observed grains of volcanic biotite that were partially replaced by complex intergrowths of chlorite, corrensite, and minor smectite layers, noting that both local layer-by-layer replacement and larger-scale dissolution-transport-precipitation processes were involved in the transition of biotite to secondary clays. The dioctahedral phase occurring as part of the fine-grained matrix of diagenetic samples is illite or mixed-layer illite/smectite, presumably derived through alteration of smectite that in turn had a source in volcanic ash, with K partly supplied by the detrital biotite and potassium feldspar. Complex intergrowths of corrensite, chlorite, and mixed layer trioctahedral materials that are directly associated with illite are therefore inferred to have formed in part by alteration of biotite and in part through dissolution of smectite. The sizes of individual, coherent chlorite packets are very small, averaging approximately 200 Å in thickness.

The transition to the anchizone is marked primarily by a decrease in the proportion of expandable smectite layers in general, and especially in the proportion of corrensite, by an increase in the average size of crystals to approximately 500 Å, and by the occurrence of a higher proportion of chlorite crystals with subhedral outlines. Smectite layers are commonly observed to terminate against chlorite layers, occasionally with terminations occurring in opposite directions in adjacent layers.

No expandable layers were observed in samples from the high grade portion of the anchizone. Chlorite was the principal trioctahedral clay that was observed, occasionally with small numbers of ~7-Å layers of berthierine. Chlorite generally occurs as relatively large crystals (averaging approximately 800 Å in thickness) that commonly have well-defined subhedral to euhedral outlines. It also occurs as packets intergrown with illite, forming thick stacks of chlorite-mica intergrowths. Various deformation strain features reflect tectonic stress, and textures generally illustrate continued adjustment of texture via dissolution and crystallization.

The epizone samples are marked by a further increase in crystal size to an average thickness of approximately 2000 Å, increased definition of crystal outlines, and a decrease in the number of defects. Although various deformation features reflect adjustment to tectonic stress, the samples are relatively homogeneous.

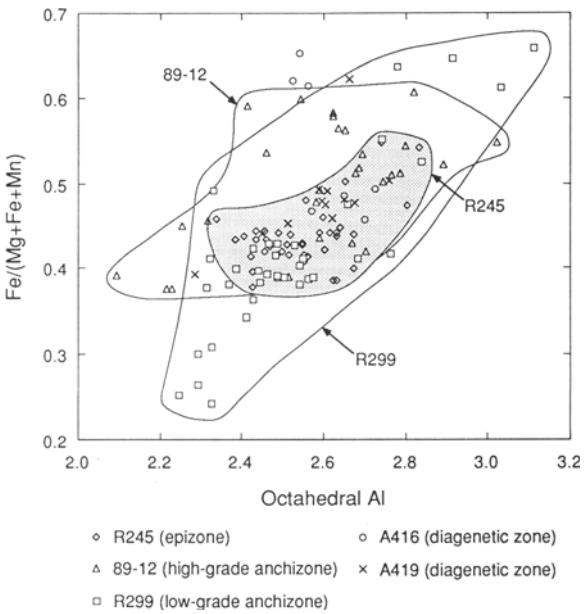

Figure 16. Plot of octahedral Al vs. Fe/(Mg + Fe + Mn) showing the compositional variation of chlorite in the Gaspé samples. The solid closing curves illustrate the compositional range of chlorite in the anchizonal and epizonal samples. The range of the epizonal chlorite is stippled.

The Gaspé sequence is thus one in which a high proportion of expandable trioctahedral layers formed with varying degrees of order with respect to chlorite, as direct replacement of volcanic detritus and by larger-scale dissolution and crystallization. These small, defect-rich crystals were gradually replaced, again by a combination of layer-by-layer replacement and dissolution and crystallization by larger crystals of defect-poor chlorite. Further changes are evident in the increase in size of chlorite and white micas, decreasing concentrations of defects, and improved definition of individual crystals. All changes are consistent with a trend from metastable, disordered phases toward a mineralogically simple system that approaches a state of equilibrium with respect both to the small number of homogeneous phases and to texture (Peacor 1992).

Compositional variation of chlorite

Figure 16 shows the relations for octahedral cations of the Gaspé chlorite. The octahedral composition also reflects the tetrahedral composition (assuming no ferric Fe) because all formulae, as normalized to anions, have nearly full octahedral occupancy; the numbers of octahedral and tetrahedral Al are therefore approximately equal. The range of octahedral Al contents is relatively small (2.1–3.1 pfu), but Fe/(Mg + Fe + Mn) varies widely. The range of variation decreases with

https://doi.org/10.1346/CCMN.1994.0420501 Published online by Cambridge University Press

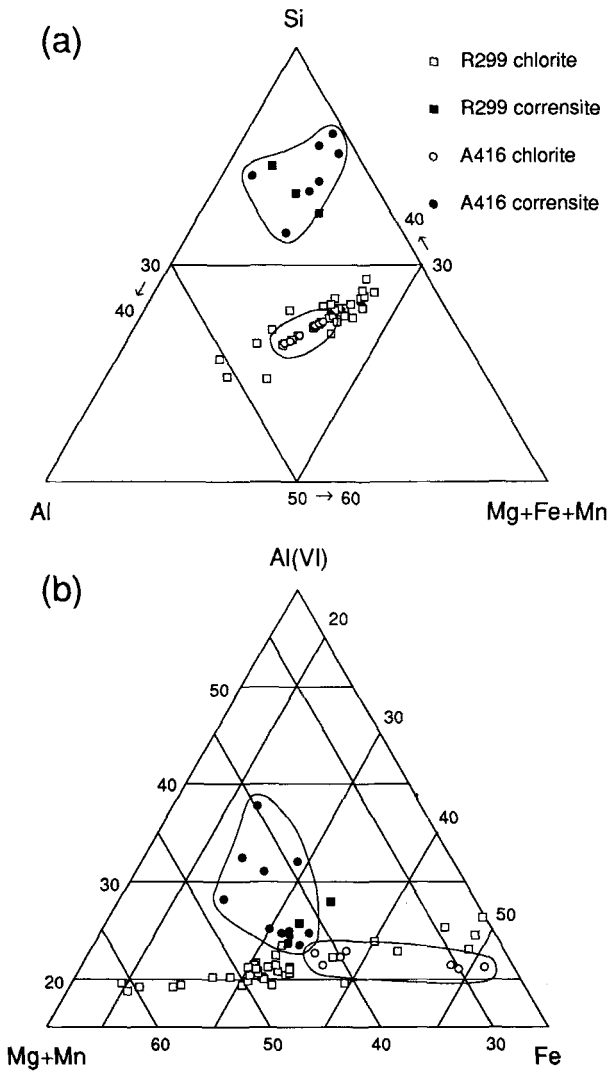

Figure 17. Ternary plots Si–Al–(Mg + Fe + Mn) and Al(VI)–(Mg + Mn)–Fe showing compositional differences between corrensite and chlorite in the diagenetic (A416) and low-grade anchizonal (R299) rocks of the Gaspé sequence. The data points for sample A416 are enclosed with solid curves.

increasing grade from the low-grade anchizone to the epizone, as consistent with the trend toward homogenization of thermodynamically stable phases described above. The limited composition range of the diagenetic chlorite (19 analyses total from two samples) appears to be an exception to the rule, but that is undoubtedly due to the limited number of analyses and a lack of analyses of the dominant small packets which are most likely to be heterogeneous.

Although data points are widely scattered, there is a general positive correlation between the Fe/(Mg + Fe + Mn) ratio and Al content of chlorite (Figure 16). Such a trend is consistent with minimization of the misfit between octahedral and tetrahedral sheets of the 2:1 layer, although other factors may also be involved (Bailey 1988). The increase in Al content would give rise to an increase and a decrease in the lateral dimensions of tetrahedral and octahedral sheets, respectively, which may require a substitution of Fe for Mg or Mn in the octahedral sheet to compensate for such changes.

Contrary to observations of many studies, the average compositions of chlorite for each grade are approximately the same and most of our chlorite analyses show nearly full trioctahedral occupancy. These characteristics are different than those of most electron microprobe analyses of low-grade chlorite, for which significant octahedral vacancies are frequently reported (Hillier and Velde 1991), a relation implying contamination by interlayered phases that occur commonly in metabasites (Shau *et al* 1990; Schiffman and Fridleifsson 1991). These relations and the lack of stable equilibrium as generally recognized (Velde and Medhioub 1988; Peacor 1992; de Caritat *et al* 1993) and demonstrated above for the Gaspé chlorite suggest that use of chlorite composition as a geothermometer in low-grade regimes (Cathelineau and Nieva 1985; Cathelineau 1988) is not warranted.

Compositional relation between coexisting corrensite and chlorite

Figures 17a and 17b are plots of Si–Al–(Mg + Fe + Mn) and Al(VI)–(Mg + Mn)–Fe compositional components, respectively, of corrensite and chlorite in samples A416 and R299. The plots show that the corrensite is more Si- and Mg-rich than the coexisting chlorite in the diagenetic sample, consistent with the general crystal-chemical relations between corrensite and chlorite in basalt alteration parageneses (Shau *et al* 1990; Shau and Peacor 1992) or in hydrothermal smectite-to-chlorite conversion sequences (Inoue *et al* 1984; Inoue 1987). The smectite-like interlayer of corrensite is defined by Si-rich tetrahedral sheets that give rise to a small interlayer net negative charge, which requires that the octahedral sheet have minimum dimensions as consistent with low Fe occupancy to minimize misfit. The analyses of corrensite and chlorite by Inoue (1985), Bettison-Varga *et al* (1991), and Inoue and Utada (1991), however, show decreased or nearly constant Fe/(Mg + Fe) ratios concomitant with an increase of Al/(Si + Al) ratios in conversions of smectite to corrensite. Bettison-Varga *et al* (1991) suggested that such an inverse chemical relation may be due to a lack of ample fluid, resulting in diverse local chemical environments and formation processes. The wide distribution of data points in Figure 17 may be a reflection of local environments, but the general crystal-chemical relations between corrensite and chlorite remain consistent for most analyses obtained for the diagenetic sample. This perhaps is because diagenesis of pelites is a slow, long-term process compared to the hydrothermal alteration of mafic rocks. The octahedral con-

tents of corrensite overlap those of the coexisting chlorite in the low-grade zone because the chlorite was formed by various formation processes discussed below.

Crystal chemistry of corrensite

The corrensite ~24-Å units in the studied samples commonly cluster together forming packets of layers interstratified with chlorite or else they occur as discrete crystals intergrown with chlorite and illite. The very common occurrence of relatively thick packets of corrensite in the lowest grade rocks clearly attests to the stability of such an ordered sequence of smectite-like and chlorite-like layers and thus to the uniqueness of corrensite relative to an assemblage of separate smectite and chlorite layers. However, assuming that chlorite layers have formed by transformation of smectite-like layers, the presence of smectite-like layers separated by small, even numbers of chlorite layers implies that consecutive smectite-like layers must have previously existed. Indeed, consecutive smectite-like layers were directly observed (Figure 9), in contrast to the observations of Shau *et al* (1990) on phyllosilicates in metabasites. Utilizing lattice-fringe images, they showed that chloritic minerals tend to occur as intergrowths of discrete chlorite and corrensite or interstratified chlorite/corrensite rather than C/S in regionally metamorphosed basalts from northern Taiwan.

Shau *et al* (1990) also suggested that corrensite has a unique structure consisting of smectite-like and chlorite-like layers and that it should be considered to be a unique phase rather than as a simple mixture of smectite and chlorite layers. Meunier *et al* (1988) and Mexias *et al* (1990) also suggested that corrensite is a thermodynamically unique phase based on mineral parageneses controlled by $f(O_2)$ and $X(CO_2)$ in carbonate and volcanoclastic rocks. A similar view was proposed by Inoue (1985) based on the stepwise transitions from smectite through corrensite to chlorite shown by XRD data in the diagenesis of pyroclastic rocks from northern Japan.

Does the observation of relations among smectite- and chlorite-like layers occurring in rocks from the Gaspé Peninsula conflict with those conclusions? Jiang (1993) showed that much of the Gaspé corrensite or C/S was formed by direct replacement of layers of detrital biotite during early diagenesis. A layer by layer replacement process is one in which initiation of replacement of individual layers by a given new layer may have little relation to the nature of adjacent layers, as opposed to the wholesale growth of layers from fluids, as in altered basalts. In addition, such low-temperature alteration of phyllosilicates commonly produces metastable mixed layers that have a wide range of complex intergrowth textures or structures (Banfield and Eggleton 1988; Jiang *et al* 1992; Bettison-Varga *et al* 1991). Indeed, Bettison-Varga *et al* (1991) and Shau and Peacor (1992) observed consecutive smectite-like layers in C/S in hydrothermally altered basaltic rocks and inferred that they were metastable alteration products formed locally in environments with limited fluid, as is the case with pelites. The relatively uncommon occurrence of adjacent smectite-like layers in rocks where corrensite is abundant is to be expected, because such metastable disorder and heterogeneity is the rule rather than the exception in such low-grade rocks (Peacor 1992). The occurrence of apparent random C/S (and chlorite/corrensite) is therefore not in conflict with the uniqueness of corrensite. Indeed, the observed high concentration of well-ordered corrensite relative to random C/S, the formation of corrensite and chlorite directly from biotite, and the crystal-chemical relations between corrensite and chlorite discussed above imply such uniqueness.

Our TEM data show that the corrensite crystals are small and frequently contain chlorite mixed layers as well as numerous defects. The chlorite packets are rather large and defect-free compared with coexisting corrensite packets. These contrasting features have been observed in other TEM studies (Shau *et al* 1990; Bettison-Varga *et al* 1991; Shau and Peacor 1992). In conjunction with the commonly observed conversion of corrensite to chlorite in many prograde sequences of low-grade rocks (Helmold and van de Kamp 1984; Chang *et al* 1986; Inoue 1987; Inoue and Utada 1991), these relations imply that corrensite may indeed be metastable relative to chlorite, just as R1 mixed-layer illite/smectite or illite forms metastably relative to white micas (Jiang *et al* 1990).

Diagenetic alteration of corrensite to chlorite

The TEM data are consistent with a prograde reaction from corrensite to chlorite. The presence of a wide range of intergrowth textures between corrensite and chlorite, including intergrowths of discrete chlorite and corrensite crystals, interstratification of packets of layers, complex mixed layering, and especially terminations of single smectite layers by chlorite layers, implies that some of the chlorite may either have formed simultaneously with corrensite as a diagenetic alteration product of precursor phases such as smectite or detrital biotite (Jiang 1993), or have originated from diagenetic alteration of corrensite. The diminution of corrensite and formation of chlorite are reconciled with an alteration sequence of trioctahedral phyllosilicates in a prograde environment (Hoffman and Hower 1979; Helmold and van de Kamp 1984; Inoue 1985, 1987; Chang *et al* 1986; Inoue and Utada 1991; Meunier *et al* 1988). At least some of the diagenetic chlorite must have originated from the corrensite. The occurrence of curved corrensite packets crosscut by straight packets of chlorite and corrensite (Figure 7) is also consistent with a replacement of corrensite by chlorite.

However, some of the chlorite crystallized directly

from pore fluids, independent of the formation of corrensite, as evidenced by the formation of euhedral to subhedral chlorite crystals in the absence of corrensite (Figure 8). Such crystals may have formed at the expense of other precursor phases such as smectite, mixed-layer illite/smectite (Hower *et al* 1976), kaolinite (Boles and Franks 1979), or berthierine (Walker and Thompson 1990). Mixed-layer illite/smectite is present in the lowest grade rock of the studied sequence and the euhedral chlorite crystals commonly are intergrown with illite. Berthierine was also observed to be intergrown with chlorite in the diagenetic rocks. These relations suggest that both berthierine and mixed-layer illite/smectite may have been the precursor phases of this type of chlorite. Alternatively, such chlorite crystals may have formed through the sequence of complete dissolution of corrensite or biotite, transport to nucleation sites, and crystallization. In any event, this type of chlorite was formed by processes different from that giving rise to the formation of chlorite-corrensite intergrowths, although we are not able to identify any compositional differences between the two types of chlorite.

Syntectonic crystallization of chloritic minerals

All samples described in this study display a variety of deformation features such as crystal bending, kinking, and inter- and intra-crystal gliding. Such features are not observed in tectonic stress-free, burial metamorphic pelite sequences (Peacor 1992). However, they are common in pelites of low grade metamorphic provinces that have been subject to tectonic stress (White and Knipe 1978) and are inferred to result from the tectonic stress to which all rocks of this study were subjected (Islam *et al* 1982; Hesse and Dalton 1991).

Adjacent crystals that display contrasting deformation properties (bending and gliding vs. little or no deformation) and have well-defined interlocking relations are common in the Gaspé samples. Such textures imply that crystal growth occurred after initiation of deformation, consistent with syntectonic metamorphism (White and Knipe 1978). Large-scale dissolution and crystallization features were commonly observed in this study, e.g., where deformed corrensite-rich packets of irregular shape were observed to be cross-cut by subhedral packets of chlorite having no smectitic layers. Dissolution of deformed, unstable phases and subsequent crystallization of undeformed relatively stable phases have been commonly observed in syntectonically metamorphosed rocks (Knipe 1979, 1981; White and Johnston 1981; Weber 1981). Knipe (1981) suggested that deformation may accelerate metamorphic reactions that cause a decrease in the total energy of a rock system. Many of the observations of this study, including truncation of bent corrensite packets by relatively straight packets of chlorite and corrensite in the hinge of microfolds (Figure 7) is consistent with such a process. Recrystallization is also an important process in the diagenesis/metamorphism of the Gaspé chlorite. Crystals were commonly observed to have coalesced by readjustment of crystal boundaries and elimination of subgrain boundaries in rocks of all grades, contributing to an increase in crystal size with increasing grade. Such processes presumably occur by local dissolution and crystallization.

The collective data suggest that deformation and dissolution/crystallization/recrystallization are locally competing processes in such tectonically stressed rocks, with crystal growth dominating at higher metamorphic grades. The chlorite crystallinity index, which is a function of crystal size, lattice strain, mixed layering, and perhaps compositional heterogeneity, is thus defined by such kinetically-controlled processes. The chlorite crystallinity index therefore should be viewed as a P, T, t- and strain-controlled parameter rather than as a simple indicator only of diagenetic or metamorphic grade.

ACKNOWLEDGMENTS

Special thanks are due to R. Hesse of McGill University for providing all samples and much supporting information. We thank E. J. Essene, B. A. van der Pluijm, L. M. Walter, W. C. Elliott, and an anonymous reviewer for their helpful reviews. This study was supported by NSF grants EAR-88-17080 and EAR-91-04565 to DRP. The scanning transmission electron microscope and scanning electron microscope utilized in this work were acquired under NSF grants EAR-87-08276 and BSR-83-14092, respectively.

REFERENCES

Ahn, J. H., and D. R. Peacor. 1985. Transmission electron microscopic study of diagenetic chlorite in Gulf Coast argillaceous sediments. *Clays & Clay Miner.* **33**: 228–236.

Ahn, J. H., and D. R. Peacor. 1986. Transmission and analytical electron microscopy of the smectite-to-illite transition. *Clays & Clay Miner.* **34**: 165–179.

Alt, J. C., T. F. Anderson, L. Bonnell, and K. Muehlenbachs. 1989. Mineralogy, chemistry, and stable isotopic compositions of hydrothermally altered sheeted dikes: ODP Hole 504B, Leg 111. *Proc. Ocean Drilling Prog., Sci. Res.* **111**: 27–39.

Alt, J. C., J. Honnorez, C. Laverne, and R. Emmermann. 1986. Hydrothermal alteration of a 1 km section through the upper oceanic crust, DSDP Hole 504B: Mineralogy, chemistry and evolution of seawater-basalt interactions. *J. Geophys. Res.* **91**: 10309–10335.

Anjos, S. C. 1986. Absence of clay diagenesis in Cretaceous-Tertiary marine shales, Campos basin, Brazil. *Clays & Clay Miner.* **34**: 424–434.

April, R. H. 1981. Trioctahedral smectite and interstratified chlorite/smectite in Jurassic strata of the Connecticut Valley. *Clays & Clay Miner.* **29**: 31–39.

Bailey, S. W. 1988. Chlorites: Structures and crystal chemistry. In *Hydrous Phyllosilicates (Exclusive of Micas), Reviews in Mineralogy, Volume 19*. S. W. Bailey, ed. Washington, D.C.: Mineralogical Society of America, 347–403.

Banfield, J. F., and R. A. Eggleton. 1988. Transmission

electron microscope study of biotite weathering. *Clays & Clay Miner.* **36**: 47–60.

Bettison, L. A., and P. Schiffman. 1988. Compositional and structural variations of phyllosilicates from the Point Sal ophiolite, California. *Amer. Mineral.* **73**: 62–76.

Bettison-Varga, L., I. D. R. Mackinnon, and P. Schiffman. 1991. Integrated TEM, XRD, and electron microprobe investigation of mixed-layer chlorite-smectite from the Point Sal ophiolite, California. *J. Metamorphic Geol.* **9**: 697–710.

Björlykke, K. 1974. Geochemical and mineralogical influence of Ordovician island arcs on epicontinental clastic sedimentation. A study of Lower Palaeozoic sedimentation in the Oslo Region, Norway. *Sedimentology* **21**: 251–272.

Boles, J. R., and S. G. Franks. 1979. Clay diagenesis in Wilcox sandstones of southwest Texas: Implications of smectite diagenesis on sandstone cementation. *J. Sediment. Petrol.* **49**: 55–70.

Brigatti, M. F., and L. Poppi. 1984. Crystal chemistry of corrensite: A review. *Clays & Clay Miner.* **32**: 391–399.

Brown, G., and G. W. Brindley. 1984. X-ray diffraction procedures for clay mineral identification. In *Crystal Structures of Clay Minerals and Their X-ray Identification.* G. W. Brindley and G. Brown, eds. London: Mineralogical Society, 305–360.

Burtner, R. L., and M. A. Warner. 1986. Relationship between illite/smectite diagenesis and hydrocarbon generation in Lower Cretaceous Mowry and Skull Creek shales of the northern Rocky Mountain area. *Clays & Clay Miner.* **34**: 390–402.

Cathelineau, M. 1988. Cation site occupancy in chlorites and illites as a function of temperature. *Clay Miner.* **23**: 471–485.

Cathelineau, M., and D. Nieva. 1985. A chlorite solid solution geothermometer. The Los Azufres (Mexico) geothermal system. *Contrib. Mineral. Petrol.* **91**: 235–244.

Chang, H. K., F. T. Mackenzie, and J. Schoonmaker. 1986. Comparisons between the diagenesis of dioctahedral and trioctahedral smectite, Brazilian offshore basins. *Clays & Clay Miner.* **34**: 407–423.

Conkin, J. E. 1986. *Chattanooga Shale in the Tennessee Valley and Ridge of Hamilton and Bledsoe Counties.* Louisville, Kentucky: Dept. Geol., Univ. Louisville, 11 pp.

Dean, R. S. 1962. *A study of St. Lawrence Lowland shales.* Ph.D. thesis, McGill University, Montreal, Canada, 236 pp.

de Caritat, P., I. Hutcheon, and J. L. Walshe. 1993. Chlorite geothermometry: A review. *Clays & Clay Miner.* **41**: 219–239.

Duba, D., and A. E. Williams-Jones. 1983. The application of illite crystallinity, organic matter reflectance, and isotopic techniques to mineral exploration: A case study in Southwestern Gaspé, Quebec. *Econ. Geol.* **78**: 1350–1363.

Enos, P. 1969. Cloridorme Formation, Middle Ordovician flysch, northern Gaspé Peninsula, Quebec. *Geol. Soc. Amer. Spec. Pap.* **117**: 66 pp.

Eslinger, E., and B. Sellars. 1981. Evidence for the formation of illite from smectite during burial metamorphism in the Belt Supergroup, Clark Fork, Idaho. *J. Sediment. Petrol.* **51**: 203–216.

Evarts, R. C., and P. Schiffman. 1983. Submarine hydrothermal metamorphism of the Del Puerto ophiolite, California. *Amer. J. Sci.* **283**: 289–340.

Faill, R. T. 1985. The Acadian orogeny and the Catskill Delta. In *The Catskill Delta.* D. L. Woodrow and W. D. Sevon, eds. *Geol. Soc. Amer. Spec. Pap.* **201**: 15–37.

Frey, M. 1978. Progressive low-grade metamorphism of a black shale formation, central Swiss Alps, with special reference to pyrophyllite and margarite bearing assemblages. *J. Petrol.* **19**: 95–135.

Helmold, K. P., and P. van de Kamp. 1984. Diagenetic mineralogy and controls on albitization and laumontite formation in Palaeogene arkoses, Santa Ynez Mountains, California. In *Clastic Diagenesis.* D. A. McDonald and R. C. Surdam, eds. *Amer. Assoc. Petroleum Geol. Mem.* **37**: 239–276.

Hesse, R., and E. Dalton. 1991. Diagenetic and low-grade metamorphic terrains of Gaspé-Peninsula related to geological structure of the Taconian and Acadian orogenic belts, Quebec Appalachians. *J. Metamorphic Geol.* **9**: 775–790.

Hillier, S., and B. Velde. 1991. Octahedral occupancy and the chemical composition of diagenetic (low-temperature) chlorites. *Clay Miner.* **26**: 149–168.

Hirsch, P., A. Howie, R. B. Nicholson, D. W. Pashley, and M. J. Whelan. 1977. *Electron Microscopy of Thin Crystals.* 2nd ed. Huntington, New York: Robert E. Krieger Publishing Co., 563 pp.

Hiscott, R. N., K. T. Pickering, and D. R. Beeden. 1986. Progressive filling of a confined Middle Ordovician foreland basin associated with the Taconic Orogeny, Quebec, Canada. In *Foreland Basins.* P. A. Allen and P. Homewood, eds. *Int'l. Assoc. Sediment. Spec. Publ.* **8**: 309–325.

Hoffman, J., and J. Hower. 1979. Clay mineral assemblages as low grade metamorphic geothermometers: Application to the thrust faulted disturbed belt of Montana, USA. In *Aspects of Diagenesis.* P. A. Scholle and P. R. Schluger, eds. *Soc. Econ. Paleontol. Mineral. Spec. Publ.* **26**: 55–79.

Hower, J., E. V. Eslinger, M. E. Hower, and E. A. Perry Jr. 1976. Mechanism of burial metamorphism of argillaceous sediments: 1. Mineralogical and chemical evidence. *Geol. Soc. Amer. Bull.* **87**: 725–737.

Hyndman, D. W. 1985. *Petrology of Igneous and Metamorphic Rocks.* New York: McGraw-Hill, 786 pp.

Inoue, A. 1985. Chemistry of corrensite: A trend in composition of trioctahedral chlorite/smectite during diagenesis. *J. Coll. Arts Sci., Chiba Univ.* **B-18**: 69–82.

Inoue, A. 1987. Conversion of smectite to chlorite by hydrothermal and diagenetic alterations, Hokuroku Kuroko mineralization area, northeast Japan. In *Proceedings of the International Clay Conference, Denver, 1985.* L. G. Schultz, H. van Olphen, and F. A. Mumpton, eds. Bloomington: The Clay Minerals Society, 158–164.

Inoue, A., and M. Utada. 1991. Smectite-to-chlorite transformation in thermally metamorphosed volcanoclastic rocks in the Kamikita area, northern Honshu, Japan. *Amer. Mineral.* **76**: 628–640.

Inoue, A., M. Utada, H. Nagata, and T. Watanabe. 1984. Conversion of trioctahedral smectite to interstratified chlorite/smectite in Pliocene acidic pyroclastic sediments of the Ohyu district, Akita Prefecture, Japan. *Clay Sci.* **6**: 103–116.

Islam, S., and R. Hesse. 1983. The P-T conditions of late-stage diagenesis and low grade metamorphism in the Taconic belt of the Gaspé Peninsula from fluid inclusions: Preliminary results. *Geol. Surv. Can., Curr. Res., Part B, Pap.* **83-1B**: 145–150.

Islam, S., R. Hesse, and A. Chagnon. 1982. Zonation of diagenesis and low-grade metamorphism in Cambro-Ordovician flysch of Gaspé Peninsula, Quebec Appalachians. *Can. Mineral.* **20**: 155–167.

Jiang, W.-T. 1993. *Diagenesis and Very Low-Grade Metamorphism of Pelitic Rocks from the Gaspé Peninsula, Quebec.* Ph.D. dissertation, University of Michigan, Ann Arbor, Michigan, 269 pp.

Jiang, W.-T., and D. R. Peacor. 1991. Transmission electron microscopic study of the kaolinitization of muscovite. *Clays & Clay Miner.* **39**: 1–13.

Jiang, W.-T., and D. R. Peacor. 1993. Formation and modification of metastable intermediate sodium potassium mica,

paragonite, and muscovite in hydrothermally altered metabasites from northern Wales. *Amer. Mineral.* **78**: 782–793.

Jiang, W.-T., E. J. Essene, and D. R. Peacor. 1990. Transmission electron microscopic study of coexisting pyrophyllite and muscovite: Direct evidence for the metastability of illite. *Clays & Clay Miner.* **38**: 225–240.

Jiang, W.-T., D. R. Peacor, and J. F. Slack. 1992. Microstructures, mixed layering, and polymorphism of chlorite and retrograde berthierine in the Kidd Creek massive sulfide deposit, Ontario. *Clays & Clay Miner.* **40**: 501–514.

Kisch, H. J. 1987. Correlation between indicators of very low-grade metamorphism. In *Low Temperature Metamorphism.* M. Frey, ed. New York: Chapman and Hall, 227–300.

Kisch, H. J. 1990. Calibration of the anchizone: A critical comparison of illite 'crystallinity' scales used for definition. *J. Metamorphic Geol.* **8**: 31–46.

Knipe, R. J. 1979. Chemical changes during slate cleavage development. *Bull. Minéral.* **102**: 206–209.

Knipe, R. J. 1981. The interaction of deformation and metamorphism in slates. *Tectonophys.* **78**: 249–272.

Lee, J. H., D. R. Peacor, D. D. Lewis, R. P. Wintsch. 1986. Evidence for syntectonic crystallization for the mudstone to slate transition at Lehigh Gap, Pennsylvania, U.S.A. *J. Struct. Geol.* **8**: 767–780.

Liou, J. G., Y. Seki, R. N. Guillemette, and H. Sakai. 1985. Compositions and parageneses of secondary minerals in the Onikobe geothermal system, Japan. *Chem. Geol.* **49**: 1–20.

Meunier, A., J.-Y. Clement, A. Bouchet, and D. Beaufort. 1988. Chlorite-calcite and corrensite-dolomite crystallization during two superimposed events of hydrothermal alteration in "Les Crêtes" granite, Vosges, France. *Can. Mineral.* **26**: 413–422.

Mexias, A., M. Formoso, A. Meunier, and D. Beaufort. 1990. Composition and crystallization of corrensite in volcanic and pyroclastic rocks of Hilário Formation, (RS) Brazil. In *Proceedings of the 9th International Clay Conference, Strasbourg, 1989.* V. C. Farmer and Y. Tardy, eds. *Sci. Géol., Mém.* **88**: 135–143.

Moore, D. M., and R. C. Reynolds Jr. 1989. *X-ray Diffraction and the Identification and Analysis of Clay Minerals.* New York: Oxford University Press, 332 pp.

Peacor, D. R. 1992. Diagenesis and low-grade metamorphism of shales and slates. In *Minerals and Reactions at the Atomic Scale: Transmission Electron Microscopy, Reviews in Mineralogy, Vol. 27.* P. R. Buseck, ed. Washington, D.C.: Mineralogical Society of America, 335–380.

Pickering, K. T. 1987. Deep-marine foreland basin and forearc sedimentation: A comparative study from the Lower Palaeozoic northern Appalachians, Quebec and Newfoundland. In *Marine Clastic Sedimentology.* J. K. Leggett and G. G. Zuffa, eds. London: Graham and Trotman, 190–211.

Pickering, K. T., and R. N. Hiscott. 1985. Contained (reflected) turbidity currents from the Middle Ordovician Cloridorme Formation, Quebec, Canada: An alternative to the antidune hypothesis. *Sedimentology* **32**: 373–394.

Pollastro, R. M., and C. E. Barker. 1986. Application of clay-mineral, vitrinite reflectance, and fluid inclusion studies to the thermal and burial history of the Pinedale anticline, Green River basin, Wyoming. In *Roles of Organic Matter in Sediment Diagenesis.* D. L. Gautier, ed. *Soc. Econ. Paleont. Mineral. Spec. Publ.* **38**: 73–83.

Quinlan, G. M., and C. Beaumont. 1984. Appalachian thrusting, lithospheric flexture, and the Palaeozoic stratigraphy of the Eastern Interior of North America. *Can. J. Earth Sci.* **21**: 973–996.

Reynolds, R. C. Jr. 1984. Interstratified clay minerals. In *Crystal Structures of Clay Minerals and Their X-ray Identification.* G. W. Brindley and G. Brown, eds. London, U.K.: Mineralogical Society, 249–303.

Reynolds, R. C. Jr. 1988. Mixed layer chlorite minerals. In *Hydrous Phyllosilicates (Exclusive of Micas), Reviews in Mineralogy, Vol. 19.* S. W. Bailey, ed. Washington D.C.: Mineralogical Society of America, 601–629.

Rheams, K. F., and L. N. Thornton. 1988. Characterization and geochemistry of Devonian oil shale, north Alabama, northwest Georgia, and south-central Tennessee: A resource evaluation. *Geol. Surv. Alabama Bull.* **128**: 1–214.

Roberson, H. E. 1988. Random mixed-layer chlorite-smectite: Does it exist? In *Abstracts, 25th Clay Minerals Society Annual Meeting,* Grand Rapids, Michigan, p. 98.

Roberson, H. E. 1989. Corrensite in hydrothermally altered oceanic rocks. In *Abstracts, 26th Clay Minerals Society Annual Meeting,* Sacramento, California, p. 59.

Roberts, B., and R. J. Merriman. 1990. Cambrian and Ordovician metabentonites and relevance to the origins of associated mudrocks in the northern sector of the Lower Palaeozoic Welsh marginal basin. *Geological Magazine* **127**: 31–43.

Robinson, D., and R. E. Bevins. 1986. Incipient metamorphism in the Lower Palaeozoic marginal basin of Wales. *J. Metamorphic Geol.* **4**: 101–113.

Schiffman, P., and G. O. Fridleifsson. 1991. The smectite-chlorite transition in drillhole NJ-15, Nesjavellir geothermal field, Iceland: XRD, BSE and electron microprobe investigations. *J. Metamorphic Geol.* **9**: 679–696.

Shau, Y.-H., and D. R. Peacor. 1992. Phyllosilicates in hydrothermally altered basalts from DSDP hole 504B, leg 83—A TEM and AEM study. *Contrib. Mineral. Petrol.* **112**: 119–133.

Shau, Y.-H., D. R. Peacor, and E. J. Essene. 1990. Corrensite and mixed-layer chlorite/corrensite in metabasalt from northern Taiwan: TEM/AEM, EPMA, XRD, and optical studies. *Contrib. Mineral. Petrol.* **105**: 123–142.

Slack, J. F., W.-T. Jiang, D. R. Peacor, and P. M. Okita. 1992. Hydrothermal and metamorphic berthierine from the Kidd Creek volcanogenic massive sulfide deposit, Timmins, Ontario. *Can. Mineral.* **30**: 1127–1142.

Šrodoń, J. 1984. X-ray powder diffraction identification of illitic materials. *Clays & Clay Miner.* **32**: 337–349.

St. Julien, P., and C. Hubert. 1975. Evolution of the Taconian orogen in the Quebec Appalachians. *Amer. J. Sci.* **275-A**: 337–362.

Suchecki, R. K., E. A. Perry Jr., and J. F. Hubert. 1977. Clay petrology of Cambro-Ordovician continental margin, Cow Head klippe, western Newfoundland. *Clays & Clay Miner.* **25**: 163–170.

Tomita, K., H. Takahashi, and T. Watanabe. 1988. Quantitative curves for mica/smectite interstratifications by X-ray powder diffraction. *Clays & Clay Miner.* **36**: 258–262.

Velde, B., and M. Medhioub. 1988. Approach to chemical equilibrium in diagenetic chlorites. *Contrib. Mineral. Petrol.* **98**: 122–127.

Vergo, N., and R. H. April. 1982. Interstratified clay minerals in contact aureoles, West Rock, Connecticut. *Clays & Clay Miner.* **30**: 237–240.

Walker, J. R., and G. R. Thompson. 1990. Structural variations in chlorite and illite in a diagenetic sequence from the Imperial Valley, California. *Clays & Clay Miner.* **38**: 315–321.

Weaver, C. E. 1989. *Clays, Muds, and Shales.* Amsterdam: Elsevier, 819 pp.

Weaver, C. E., P. B. Highsmith, and J. M. Wampler. 1984. Chlorite. In *Shale-Slate Metamorphism in Southern Appalachians.* Amsterdam: C. E. Weaver and Associates, Elsevier, 99–139.

Weber, K. 1981. Kinematic and metamorphic aspects of

cleavage formation in very low-grade metamorphic slates. *Tectonophys.* **78**: 291–306.

Whalen, J. B. 1985. The McGerrigle plutonic complex, Gaspé, Quebec: Evidence of magma mixing and hybridization. *Geol. Surv. Can., Curr. Res., Part A, Pap.* **85-1A**: 795–800.

White, S. H., and D. C. Johnston. 1981. A microstructural and microchemical study of cleavage lamellae in a slate. *J. Struct. Geol.* **3**: 279–290.

White, S. H., and R. J. Knipe. 1978. Microstructural variation of an axial plane cleavage around a fold—A H.V.E.M. study. *Tectonophys.* **39**: 355–381.

Williams, H., and R. D. Hatcher. 1983. Appalachian suspect terranes. In *Contributions to the Tectonics and Geophysics of Mountain Chains.* R. D. Hatcher, H. Williams, and I. Zietz, eds. *Geol. Soc. Amer. Mem.* **158**: 33–53.

(Received 25 June 1993; accepted 28 March 1994; Ms. 2390)